Meteorological predictions for 2003 Mars Exploration Rover high-priority landing sites

Scot C. R. Rafkin and T. I. Michaels

Department of Space Studies, Southwest Research Institute, Boulder, Colorado, USA

Received 9 December 2002; revised 29 April 2003; accepted 9 May 2003; published 24 October 2003.

[1] The Mars Regional Atmospheric Modeling System is used to predict meteorological conditions that are likely to be encountered by the Mars Exploration Rovers at several proposed landing sites during entry, descent, and landing. Seven areas, five of which contain specific high-priority landing ellipses, are investigated: Hematite (two sites), Isidis Planitia, Elysium Planitia (two sites), Valles Marineris, and Gusev Crater. The last two locations are in regions of extreme topography, and the local and regional thermal circulations that result are equally extreme. Horizontal wind speeds near the floor of Valles Marineris exceed 50 ms^{-1}. Vertical velocities near the walls exceed 40 ms^{-1} and penetrate 10 km in altitude above the rim of the canyon. Thermal convection is suppressed within Valles Marineris by subsidence that forms in response to the upslope flows along the canyon walls. Wind magnitudes at Gusev crater are approximately one third of those at the canyon, but horizontal wind shear is greater. Deep convective thermals are noted at the relatively flat Hematite site, where 10 ms^{-1} updrafts rising to heights of 5 km are not uncommon during the midafternoon. Linearly organized convective updrafts superimposed on upslope circulations dominate over most of Isidis Planitia. Hexagonal and linearly organized convection predominates at Elysium Planitia. Afternoon circulations at all sites pose some risk (significant risk in some cases) to entry, descent, and landing. Most of the atmospheric hazards are not evident in current observational data and general circulation model simulations and can only be ascertained through mesoscale modeling of the region. *INDEX TERMS:* 6225 Planetology: Solar System Objects: Mars; 0343 Atmospheric Composition and Structure: Planetary atmospheres (5405, 5407, 5409, 5704, 5705, 5707); 3329 Meteorology and Atmospheric Dynamics: Mesoscale meteorology; 3346 Meteorology and Atmospheric Dynamics: Planetary meteorology (5445, 5739); 3334 Meteorology and Atmospheric Dynamics: Middle atmosphere dynamics (0341, 0342); *KEYWORDS:* Mars, atmosphere, mesoscale, modeling, meteorology, Mars Exploration Rover

Citation: Rafkin, S. C. R., and T. I. Michaels, Meteorological predictions for 2003 Mars Exploration Rover high-priority landing sites, *J. Geophys. Res.*, *108*(E12), 8091, doi:10.1029/2002JE002027, 2003.

1. Introduction

[2] The Mars Exploration Rovers utilize an entry, descent, and landing (EDL) system similar to that of the Mars Pathfinder spacecraft (Figure 1). The spacecraft becomes increasingly influenced by the mean wind and wind shear as it descends through the lowest scale height of the atmosphere [see *Kass et al.*, 2003 (hereinafter referred to as K03); *Crisp et al.*, 2003]. At approximately 11 km above ground level (AGL), a parachute is deployed to slow the vehicle. Shortly thereafter, the heatshield separates and a bridle is lowered with the lander system tethered to the end. A radar ground acquisition system operates from about 10 to 18 s before impact. The rate of descent and distance to the surface is measured during this period. Air bags surrounding the rover at the end of the tether are inflated at approximately 10 s before impact, and retrorockets and horizontal rockets fire at 7 s before impact using a firing solution based on extrapolation of data from the ground acquisition radar and attitude information from gyroscopes. The air bags containing the rover are separated from the bridle approximately 3 s before impact, after which the bags impact the ground and bounce and roll to a stop.

[3] Vertical shear of the horizontal wind can induce unwanted oscillations of the three-body EDL system (parachute, rockets, lander). There are two modes of oscillation. The first is excited by wavelengths in the range of 400 m to 1 km (the so-called "evil mode" of the system). The second mode is excited by shear with wavelengths of approximately 1.5 km. The evil mode is difficult to damp via the rockets, and in some cases, may actually be further excited by the rocket impulse. Further information about spacecraft performance and its response to the environmental winds is given by *Crisp et al.* [2003].

[4] Vertical variations of the vertical wind can also be hazardous. The firing solution for the retrorockets is obtained through extrapolation of radar data to the surface.

0148-0227/03/2002JE002027$09.00

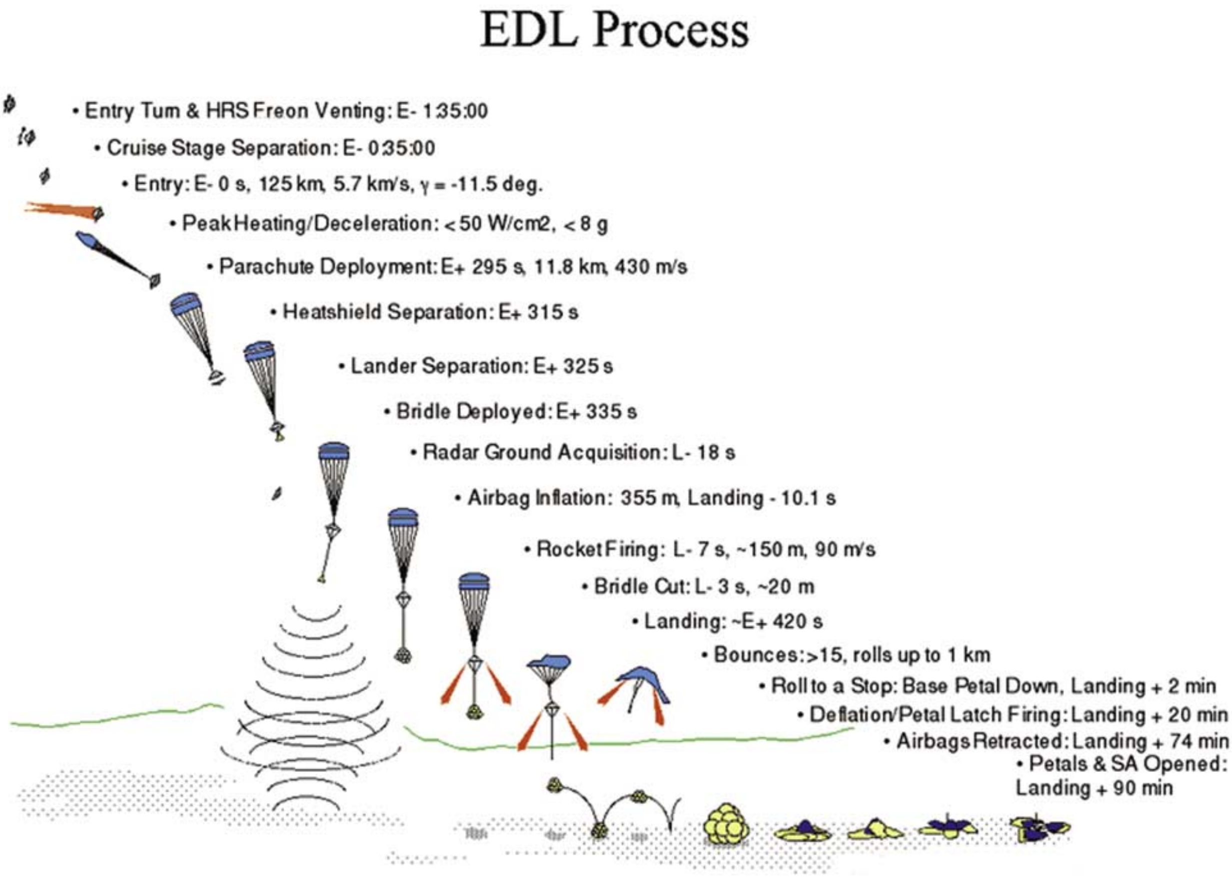

Figure 1. Entry, descent, and landing scenario for the MER spacecraft. Image Credit: JPL MER Science Team.

Extrapolation errors can result in erroneous rocket thrust calculations. Excess thrust would cause the spacecraft to obtain a zero velocity too far above the surface (and thus impact the surface at a potentially damaging velocity). Too little thrust might prevent the spacecraft from slowing sufficiently before impact.

[5] Mean wind becomes important in the last phase of descent, as the air bag system will impact the ground with a horizontal velocity approximately equal to the mean wind speed over the lowest few hundred meters to one kilometer of atmosphere. The critical horizontal speed is approximately 16 ms^{-1}. Impacts above this threshold are increasingly likely to damage the air bags and potentially the rovers, instruments, and deployment mechanisms contained within the protective bags.

[6] Five locations (those with defined landing ellipses) have been identified as possible landing sites (Figure 2). These sites are Hematite (ellipses TM20B2 and TM10A2), Elysium Planitia (EP78B2), Isidis Planitia (IP84A2 and IP96B2), Valles Marineris Melas Chasma (VM53A2 and VM53B2), and Gusev crater (EP55A2). Two additional sites with unspecified ellipses are located east of the Hematite site (referred to as ‘‘East of Hematite’’) and on the southeastern edge of Elysium Planitia (referred to as ‘‘Elysium Edge’’).

[7] Little attention was given to potential wind hazards prior to selecting the potential landing sites, although there was so little knowledge of the local meteorology at the sites that little more could be done than to speculate. Predictions from general circulation models (GCMs) were available, but the utility of these data in regions of complex topography is dubious. Winds derived from observed thermal fields (e.g., TES and Radio Science) are not of sufficient spatial or temporal resolution.

[8] In an effort to better understand the atmospheric circulations of the landing sites, and in order to provide guidance to the landing site selection team, the Mars Regional Atmospheric Modeling System (MRAMS) was applied to the seven landing sites (five of which have defined ellipses) using nested grids with a spacing of 1.5 km or less on the innermost grid that is centered over the landing ellipse. MRAMS is ideally suited for the investigation; the model is explicitly designed to simulate Mars' atmospheric circulations at the mesoscale and smaller with realistic, high-resolution surface properties [*Rafkin et al.*, 2001, 2002].

[9] The data from these simulations were provided to the MER team at the Jet Propulsion Laboratory. K03 discuss the use of these data in quantitatively assessing atmospheric hazards and the impact of the atmosphere on spacecraft performance. Although the meteorology outside the EDL time period of many of the landing sites is interesting, the focus in this paper is during the time window for landing:

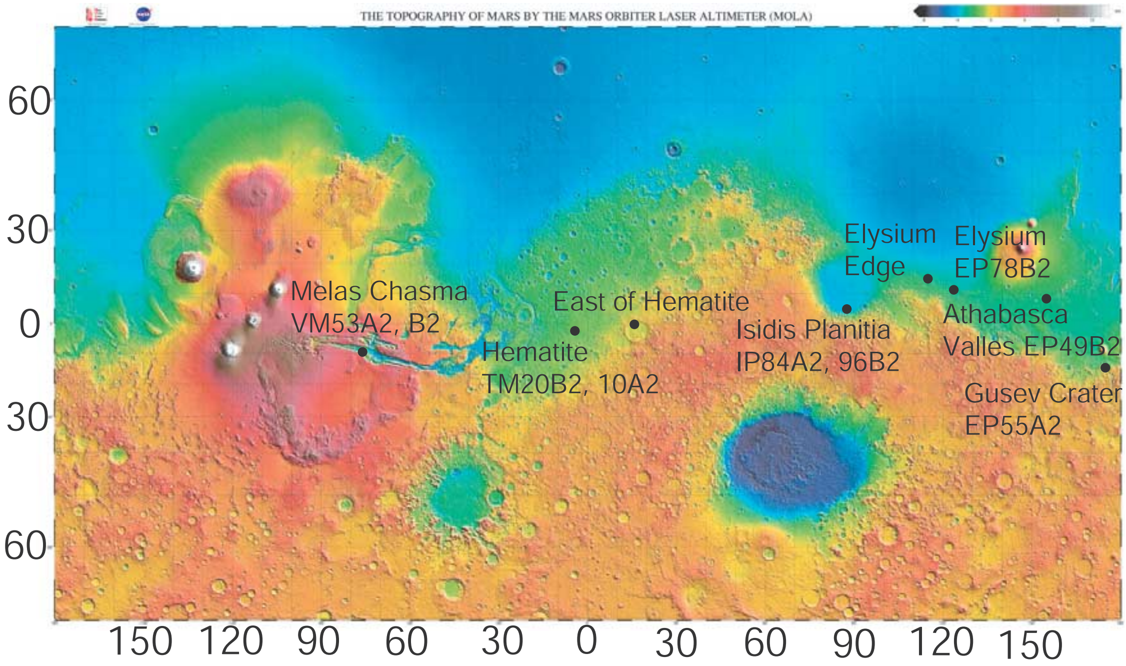

Figure 2. Potential landing locations modeled by MRAMS (black dots). When coincident with a landing ellipse, the ellipse identification label is given. Background map is shaded topographic relief as measured by the Mars Orbiter Laser Altimeter (courtesy of MOLA Science Team).

roughly 1100–1600 local time. The landing window was chosen so that communication with the spacecraft could be maintained throughout the EDL process.

2. Numerical Experiment Design

[10] Five, two-way nested [*Pielke et al.*, 1992] numerical grids were used in each of the landing site simulations. The outermost grids are as large as feasible given the constraints of computational power and the goal of keeping large topographic gradients along the boundaries to a minimum. As pointed out by *Tyler et al.* [2002], hemispheric outer domains that cross the equator are desirable in order to minimize reflections and spurious atmospheric tidal wave activity. The outermost grids were constructed with this in mind.

[11] The horizontal grid spacings on each grid are 240, 60, 15, 5, and 1.67 km, respectively. All the grids have the same vertical grid configuration. The lowest level vertical grid spacing of 30 m is gradually stretched to a maximum spacing of 1000 m. The spacing does not exceed 100 m in the lowest 1 km, and does not exceed 400 m in the lowest 4 km. The lowest model level is $\approx$14 m above the ground. The model top is typically at $\approx$40 km, although depending on the topography, some domains are higher. The total number of vertical grid points varies from 56 to 69.

[12] The selection of the vertical grid spacing resulted from several important considerations. First, the integration time step for nonhydrostatic models is closely coupled to the thickness of the lower layers. Using a lowest model thickness of one to two meters would have a required a time step so small (fractions of a second) that the simulations would have become impractical. Secondly, the MER team requested that we try to provide model layer thicknesses of no more than one to two hundred meters within the boundary layer in order to facilitate the spectral analysis of the shear profile. This request, coupled with the numerical stability constraint not to vertically stretch the grid beyond a geometric factor of about 1.2 led to the above configuration. Vertical spacing starting at a few meters would have required the use of more than 100 levels due to the geometric stretching requirement. While a 14 m lowest level is greater than what is typically used, it is probably sufficient for the task at hand where the greatest concern is in the heart of the convective boundary layer.

[13] All the experiments are initialized with data from simulation 9974 of the NASA Ames General Circulation Model climate catalog. Time-dependent boundary conditions are also supplied from these data at intervals of 1/16th of a sol. The dust opacity for this simulation is fixed at 0.30 at 611 Pa. Surface properties are obtained from TES thermal inertia and albedo data sets binned at 1/8th of a degree, and from MOLA topography binned at 1/32nd of a degree.

[14] Each simulation was started at or slightly before local sunrise at each landing site at areocentric solar longitude L_s=320°. All the experiments were integrated for a minimum of three sols. The first sol may be regarded as "spin-up", however the circulation patterns are highly repeatable from sol to sol beginning within a few hours of initialization.

3. Landing Site Meteorology at EDL Time

3.1. Gusev Crater

[15] Gusev Crater is approximately 200 km in diameter and is located at the southernmost end of Amazonis Planitia along the north-south topographic dichotomy. The southern end of the crater has an outflow channel that extends to the southeast. A volcanic cone 300 km to the north rises 5 km above the surrounding plains. Overall, the topography of the area rises toward the southern highlands.

[16] The large-scale conditions at Gusev Crater (Figure 3) show that the landing site is on the southern edge of a weak

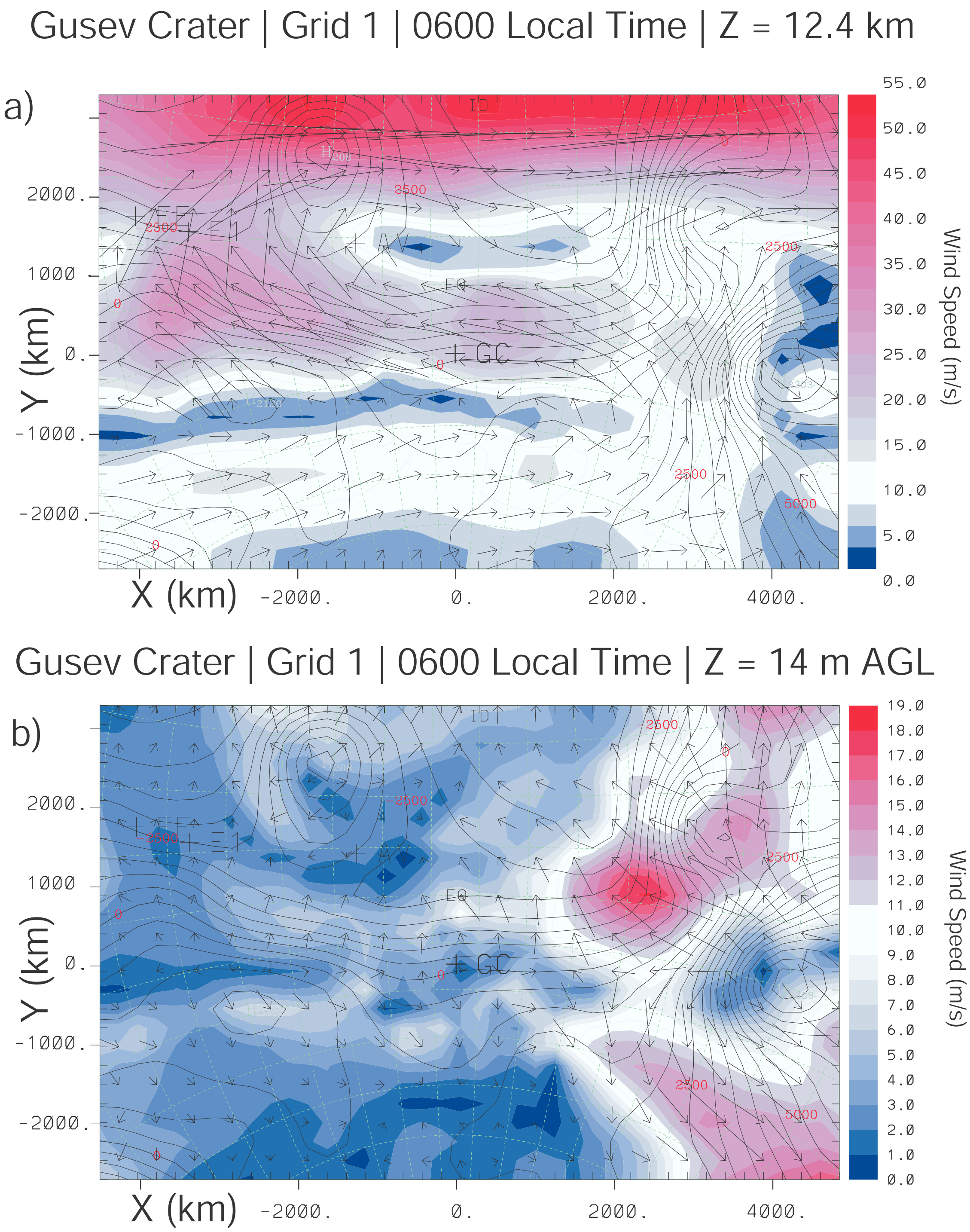

Figure 3. (a) Upper-level (12.4 km) and (b) near-surface (14 m) atmospheric circulation patterns as seen on the first computational grid. Wind speed is shaded, topography contoured. Vectors indicate wind direction and the vector length is proportional to wind speed. The center of the landing ellipse is marked with a cross and labeled GC.

upper-level easterly jet. The easterly winds weaken dramatically below approximately 11 km in altitude (all altitudes are with respect to 0 m in the MOLA data set unless otherwise specified). Winds near the surface show a distinct divergence pattern corresponding roughly to the north-south topographic dichotomy. At the time shown in Figure 3 (0600 local time at Gusev), katabatic winds emanating from the Tharsis region are evident to the east.

[17] The large-scale, low-level circulations are quickly modulated by the topography and topographically induced thermal circulations once the sun rises. A general pattern of near-surface winds diverging from the center of the crater and flowing out and up the crater walls is established (Figure 4a). Winds also flow up the outer slopes of the crater to create low-level convergence boundaries along the crater rim. The rim convergence boundaries form where

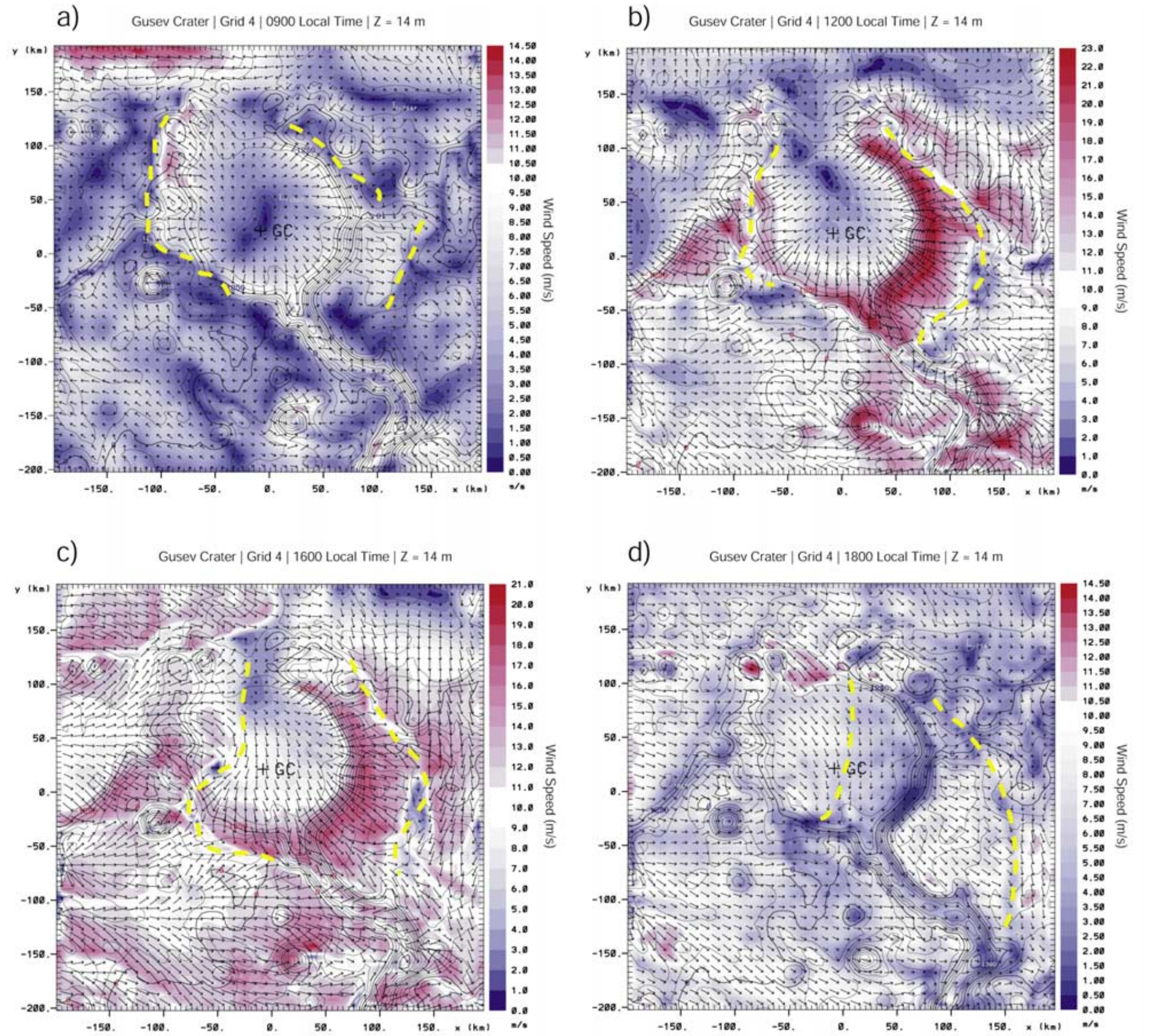

Figure 4. Atmospheric circulation (14 m) at different local times of the sol at Gusev Crater as seen on the fourth nested grid. Annotations are as in Figure 3. The daytime upslope patterns are noted in each panel. Convergence boundaries (dashed yellow) develop along the crater rim before 0900 (a). By noon (b), the boundaries are intense, but are shifted off the rim due to the mean wind and forcing from the approaching tide. At 1600 (c), the western boundary begins to move across the crater floor. By 1800 (d), the western boundary has propagated halfway through the crater.

the inner-crater winds collide with the upslope outer-crater winds.

[18] Around 1200 local time, the approach of the thermal tide from the east accelerates the low-level westerly winds, which have two important effects on the circulation. First, it causes the rim convergence boundaries to migrate toward the east with respect to the ridge of the crater rim. Second, it strengthens the upslope flow along the interior of the eastern crater rim. The strongest afternoon near-surface winds (>20 ms^{-1}) are found along the eastern rim due to the juxtaposition of the upslope thermal circulation and the tidal forcing.

[19] The western convergence boundary moves through the crater during the midafternoon to late afternoon, and the passage and location of this boundary is potentially of vital importance to EDL, as it represents a time of rapidly changing winds, enhanced vertical velocity, and wind shear. As shown in Figure 4b, the convergence boundary is displaced to the east by 1200 local time. There is little movement through 1400. By 1600, the western boundary has propagated through the eastern third of crater, and the eastern boundary is located over 50 km to the east of the eastern crater rim (Figure 4c). Although the tidal forcing has moved westward by this time, the inner western rim of the crater is now receiving significantly reduced solar insolation, and the outer western rim and inner eastern rim are receiving relatively high insolation due their aspect with respect to the sun. The net effect is an increase of low-level westerly momentum that pushes the boundary across the crater. By 1800, the boundary has moved through half the

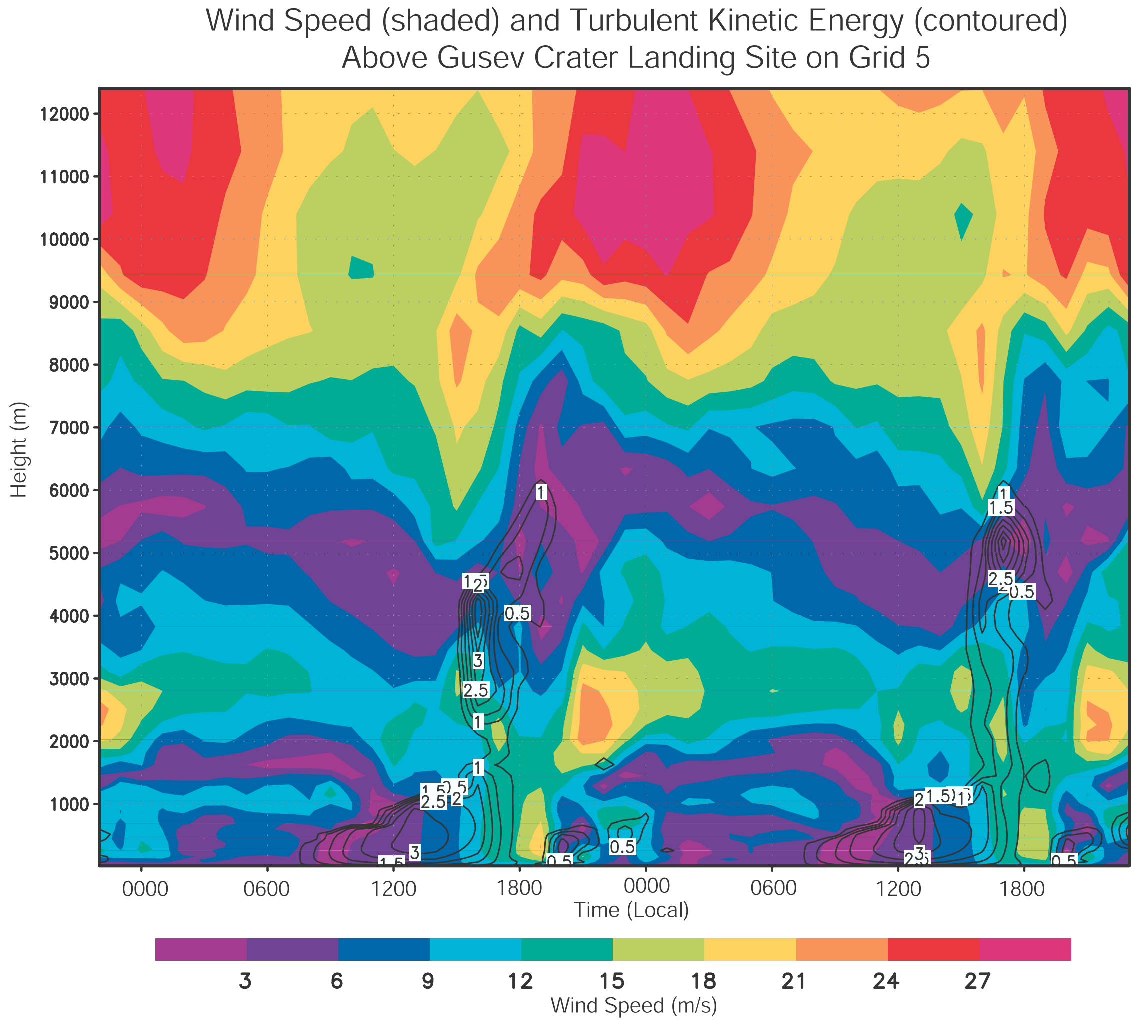

Figure 5. Time-height cross section of wind speed (shaded) and subgrid-scale turbulent kinetic energy (m^2s^{-2}, contoured) predicted on the fifth nested grid at the center of the Gusev Crater landing ellipse.

crater, although the convergence pattern has weakened (Figure 4d). Shortly thereafter, downslope (katabatic) winds develop along the inner eastern rim and undercut the relatively warmer westerly wind air mass (not shown).

[20] A time-height cross section of MRAMS wind speed and subgrid-scale turbulent kinetic energy (TKE) above the Gusev crater landing site over approximately a two sol period is shown in Figure 5. The basic diurnal pattern is repeatable. Winds in the lowest few hundred meters increase in magnitude through the afternoon and peak in the early evening at speeds in excess of 20 ms^{-1}. A layer of strong winds approximately 2 km deep lies above the weak surface winds. The maximum wind speed in this layer is about 25 ms^{-1} at 2.5 km above ground level (AGL) occurring at roughly 2200 local time. Yet another layer of weak winds is found roughly between 4 and 7 km AGL. The maximum height of this layer is found in the early evening and gradually descends in altitude over time before rising abruptly again at 1800 local time. A region of strong wind shear is found between approximately 8 and 9 km, which represents the transition between the weak winds below and easterly jet above.

[21] TKE provides a proxy for estimating the depth of the convective boundary layer, which remains remarkably shallow for most of the day. At approximately 1600 local time, an elevated layer of TKE appears, and is associated with the approach and passage of the western convergence boundary. The low-level maximum at approximately 2100 local time signifies the passage of the downslope flow from the eastern crater rim.

3.2. Valles Marineris Melas Chasma

[22] The meteorology at the Valles Marineris landing site is strongly controlled by topography just as it is at Gusev Crater. Thermal circulations along the canyon and especially across the canyon dominate the wind field. Also, there is a strong interaction between the tide and the local slope flows. However, the scale of the canyon, and the linear rather than circular nature of the topography result in significant differences between Valles Marineris and Gusev Crater. First, the canyon can strongly channel the atmospheric flow, and because the canyon runs roughly east-west, the tidal wind signal is amplified by the canyon. Second, there is positive feedback between the cross-canyon thermal circulation and the radiative heating of the air within the canyon. Radiative heating drives the thermal circulation, and the thermal circulation leads to stronger than expected radiative heating by forcing air parcels to

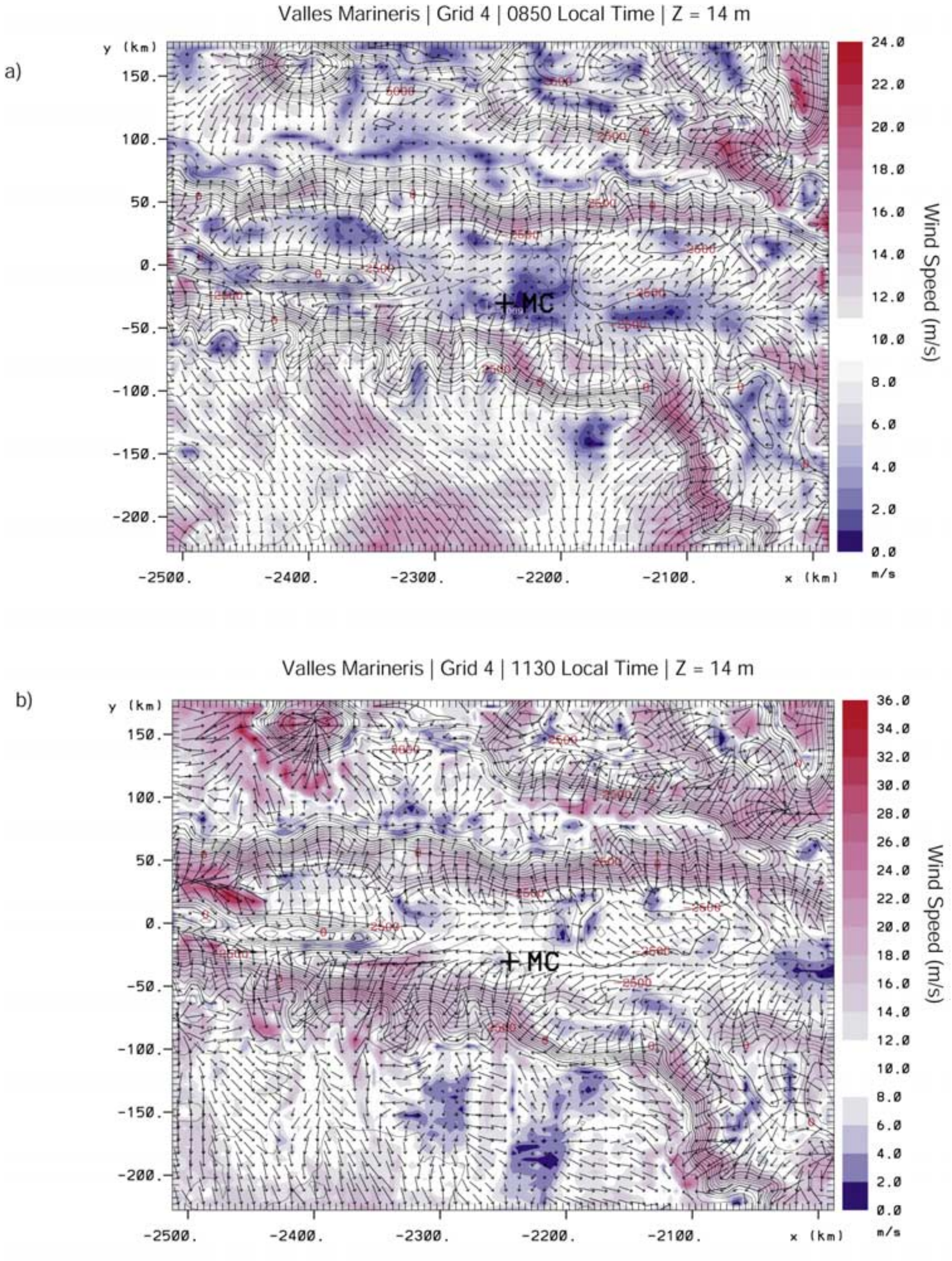

Figure 6. As in Figure 4, but for the fourth nested grid centered at the Valles Marineris (VM) landing site and at the following local times: (a) 0850, (b) 1130, and (c) 1410. Note the strong easterlies that develop by 1410.

remain longer than they otherwise would in the intense radiative heating zone near the surface. This feedback mechanism does not have any direct impact on MER, but it is interesting enough that it is worth noting.

[23] The large-scale circulation in the western half of the canyon during the morning and early afternoon is dominated by westerly surface winds reinforced by drainage winds from the Tharsis plateau (Figure 6a). The surface winds in the canyon floor flow down the large-scale topographic gradient to the east generally at less than 10 ms^{-1}. There is also pronounced cross-canyon flow; the radiatively warming air flows away from the central axis of the canyon toward and eventually up the canyon walls.

[24] As the sol progresses, the along-canyon flow slowly reverses direction. Tharsis is now warming, curtailing the production of katabatic flows from the plateau. However, the approach of the thermal tide from the east, and the corresponding low pressure, tends to increase the westerly momentum. Consequently, although thermal considerations would suggest moderate upslope winds along the canyon and toward Tharsis, the actual upslope winds generally remain below 10 ms^{-1} during the early afternoon due to opposition by the tidal forcing (Figure 6b).

[25] Once the tide passes the landing site, there is constructive interference between the upslope thermal circulation and the tide. Easterly winds increase rapidly. By

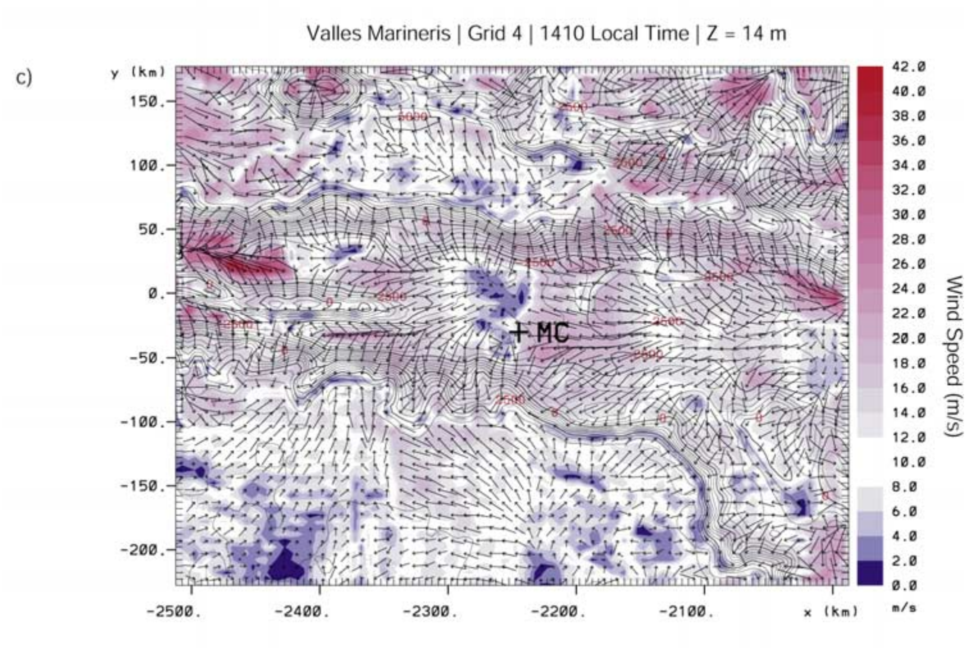

Figure 6. (continued)

approximately 1400 local time, there are broad swaths of canyon floor where the near surface wind speed is in excess of 25 ms^{-1} (Figure 6c). This situation persists through the rest of the afternoon.

[26] The spatial variations of wind speed are closely tied to the topography. The lowest elevations within in the canyon tend to have the weakest winds, especially in the lee of topographic barriers such as hills. Higher elevations are exposed to the airflow higher in the boundary layer where surface friction effects are reduced and wind speeds are consequentially greater.

[27] The proposed landing site is located on the eastern slope of a topographic bowl in the center of the valley. Consequently, the location is near a wind-sheltered area, and the local upslope flow out of the bowl tends to oppose the broader-scale upslope canyon circulation (Figure 7a). An east-west cross section through the landing site (Figure 7b) shows that although the winds tend to decrease toward the lower topography, the flow becomes highly turbulent, most likely as a result of shear-driven, rotor-like overturning. Also, note the peak wind speeds in the upslope canyon flow are in excess of 35 ms^{-1} a few hundred meters from the floor where surface friction effects have diminished.

[28] Afternoon easterly flow is enhanced by the channeling effect of the canyon, and by the return-flow-induced subsident inversion in the central interior of the canyon. The canyon and inversion conspire to produce a Bernoulli effect that accelerates the air (Figure 8).

[29] Cross-canyon flow increases in strength from the early morning hours into the late afternoon. Low-level air moves away from the central axis of the canyon toward the canyon walls. Importantly, as the air radiatively warms it does not rise and move away from the surface. It is prevented from doing so by increased static stability aloft and by the subsident return circulation. Once at the canyon walls, the air is vented out of the canyon in updrafts exceeding 40 ms^{-1}. These updrafts penetrate 10 km or more above the rim of the canyon. Air from aloft sinks into the center of the canyon, as required by mass continuity (Figure 8).

[30] Violent venting of air from the canyon is a result of the air becoming radiatively super-heated; the temperature exceeds the radiative-convective temperature. The warmest air is located along the wall of the canyon just below the rim, as this air has undergone the greatest heating due to its long residence time near the surface. Such a trajectory is only possible because of the interaction between the thermal circulation within the canyon and radiative processes. The large upward mass flux driven by the superheated air produces compensating subsidence in the center of the canyon that is stronger than it otherwise would be. Consequently, the subsident inversion and capping of thermal convection is increased, which reinforces the tendency of air to remain in the near-surface radiative heating zone, which results in a strong mesoscale circulation response and increased subsidence.

3.3. Hematite and East of Hematite

[31] The Hematite landing site is located in the weakest part of the topographic gradient dividing the northern plains and southern highlands. It is approximately 1000 km due east of the easternmost portion of Valles Marineris. As is true of most of the sites, the equatorial location is in a broad, low-level, large-scale wind shear zone. However, due to the presence of the Tharsis plateau to the west, a southward flowing boundary current is present to the west (which also contributes to the Hadley cell circulation). A counterclockwise-rotating gyre that is most evident in the lowest several kilometers (Figure 9a) results from the juxtaposition of the large-scale circulation and the boundary current. The Hematite site is located near the circulation center where wind speeds are generally well below 10 ms^{-1}. During the afternoon, the mean winds are easterly or northeasterly near the surface (Figure 9a). Above about 5 km, the winds are

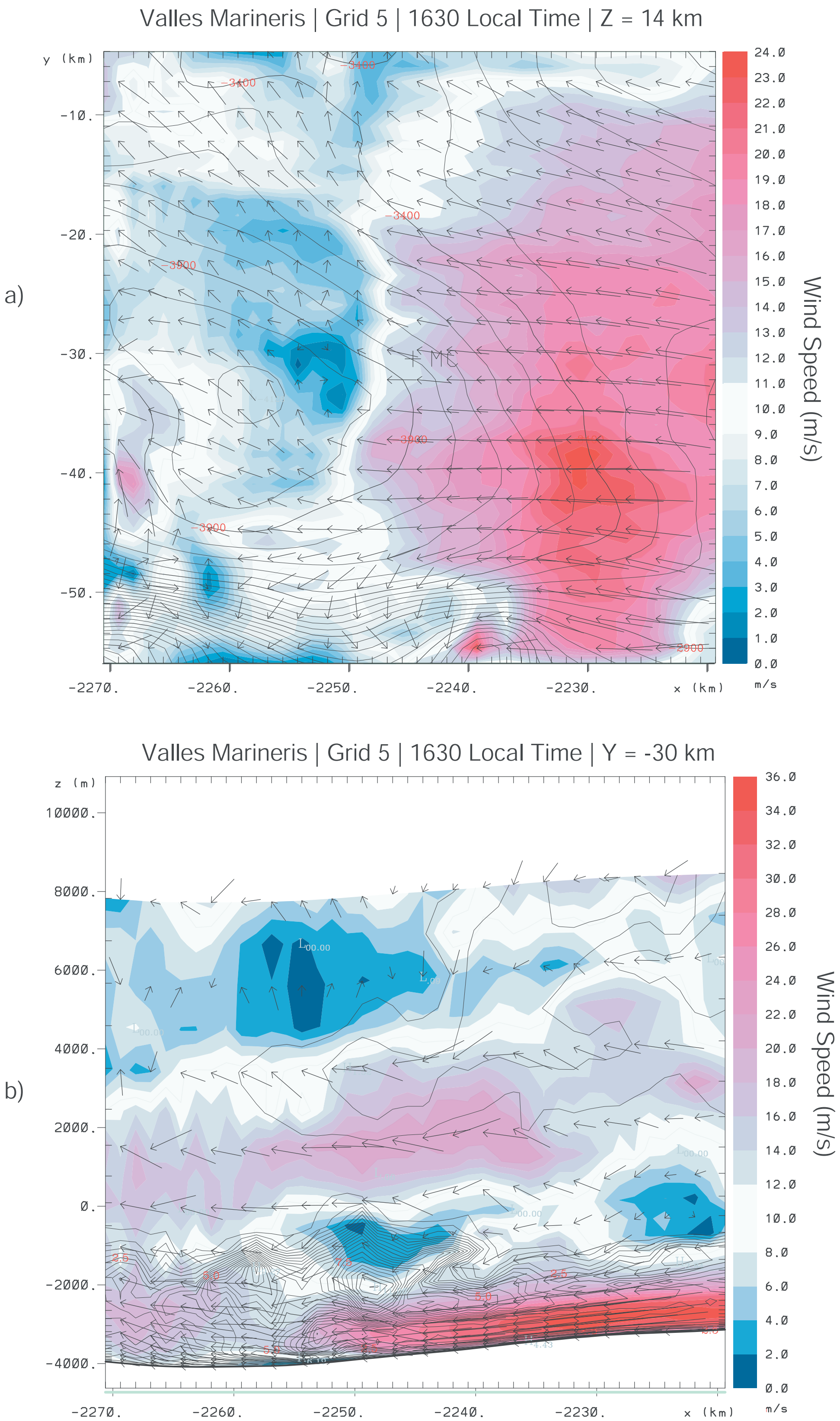

Figure 7. (a) Near-surface winds (14 m) predicted on the fifth nested grid. Wind speed is shaded and topography is contoured. (b) West-to-east vertical cross section on the fifth nested grid. Wind speed is shaded and subgrid-scale TKE is contoured.

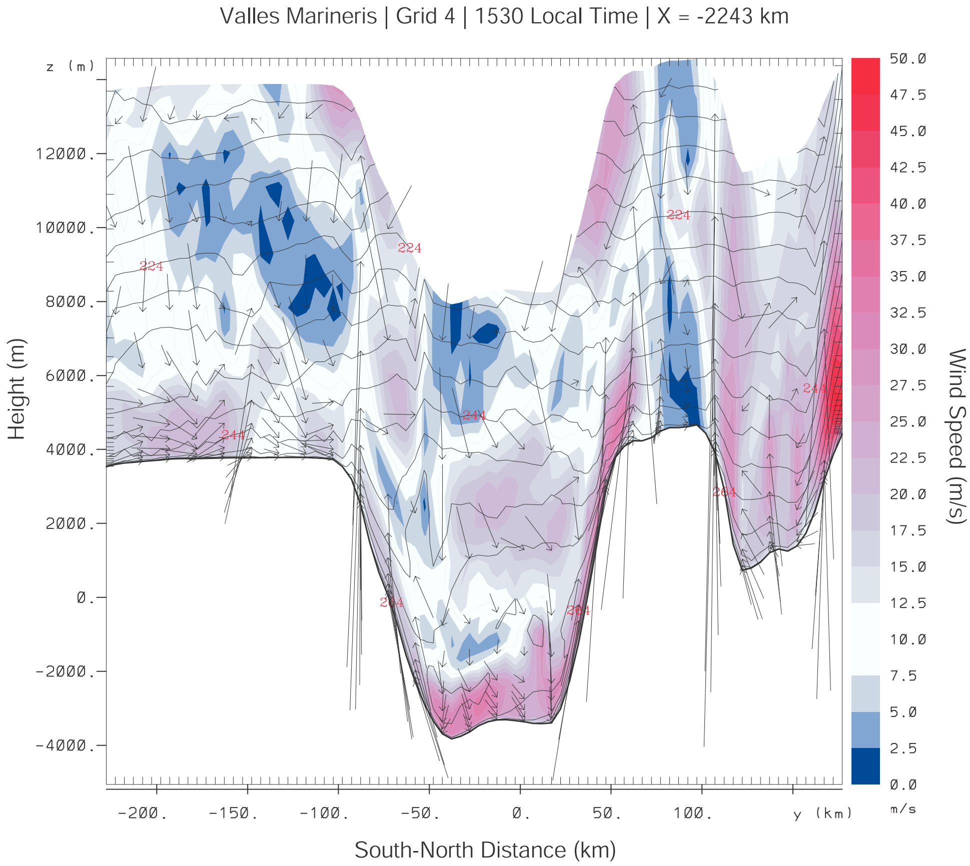

Figure 8. A south-to-north vertical cross section across the canyon centered at the landing site. Wind speed is shaded, temperature (K) is contoured. Upslope winds are noted along the canyon walls, and compensating subsidence is evident in the center of the canyon.

easterly or southeasterly (not shown). At 10 km and higher, the easterly tropical jet is present (as it was at Gusev Crater) (Figure 9b), and air flows northward to the east of Tharsis (which contributes to the poleward branch of the Hadley cell). The middle-latitude westerlies 1500 km to the north are well pronounced.

[32] The structure of the boundary layer changes drastically during the daylight hours. A low-level jet quickly begins to dissipate as the nocturnal inversion is mixed away. By noon, the winds below the upper-level easterly jet are less than 10 ms^{-1}, and thermal circulations begin to develop. The convective boundary layer grows in depth to between 4 and 5 km at 1300, and in excess of 8 km by 1500 (Figure 10). The thermals penetrate to just below the easterly jet and excite gravity waves that produce noticeable structure within and above the jet.

[33] There is organization to the convection. The thermal updrafts are initially organized in a quasi-linear pattern, first excited downwind of the two craters in the eastern domain of grid five (Figure 11a). Near-surface winds converge as the air accelerates into the updrafts. Over time, the linear features begin to intersect and exhibit a hexagonal structure (Figure 11b). Concomitantly, the near-surface flow becomes increasingly dominated by a divergent wind pattern generated by the thermal downdrafts. Low wind speeds are coincident with the centers of divergence. The size of the hexagonal cells also increases with time. Similar convective patterns were noted in the large-eddy simulations conducted by T. I. Michaels and S. C. R. Rafkin (Large eddy simulation of atmospheric convection on Mars, submitted to *Quarterly Journal of the Royal Meteorological Society*, 2002) (hereinafter referred to as Michaels and Rafkin, submitted manuscript, 2002), *Michaels* [2002], and *Rafkin et al.* [2001], which also showed that the convective patterns provide an environment conducive for dust devils.

[34] The boundaries that define the convective cells are continually evolving with time. As a thermal rises and generates a corresponding downdraft, a new convergent boundary that feeds into the next generation of thermals arises, and the old boundary associated with the original thermal dissipates. The convection decreases in intensity beginning near 1600 local time, coincident in time with the decrease in net radiative heating.

[35] The weak background wind field during the afternoon is almost completely masked by the more turbulent thermal circulations. The convective circulations produce perturbations on the mean wind that are the same order of magnitude as the mean wind itself. However, an animation of the wind fields shows that the hexagonal structures are slowly advected westward with the mean flow.

[36] A second simulation centered to the east of the Hematite site (0°N, 15°E) was also performed. This simulation, named "East of Hematite" was requested upon investigation of Mars GCM solutions that showed the location to have relatively low winds. It is not associated with a particular landing ellipse.

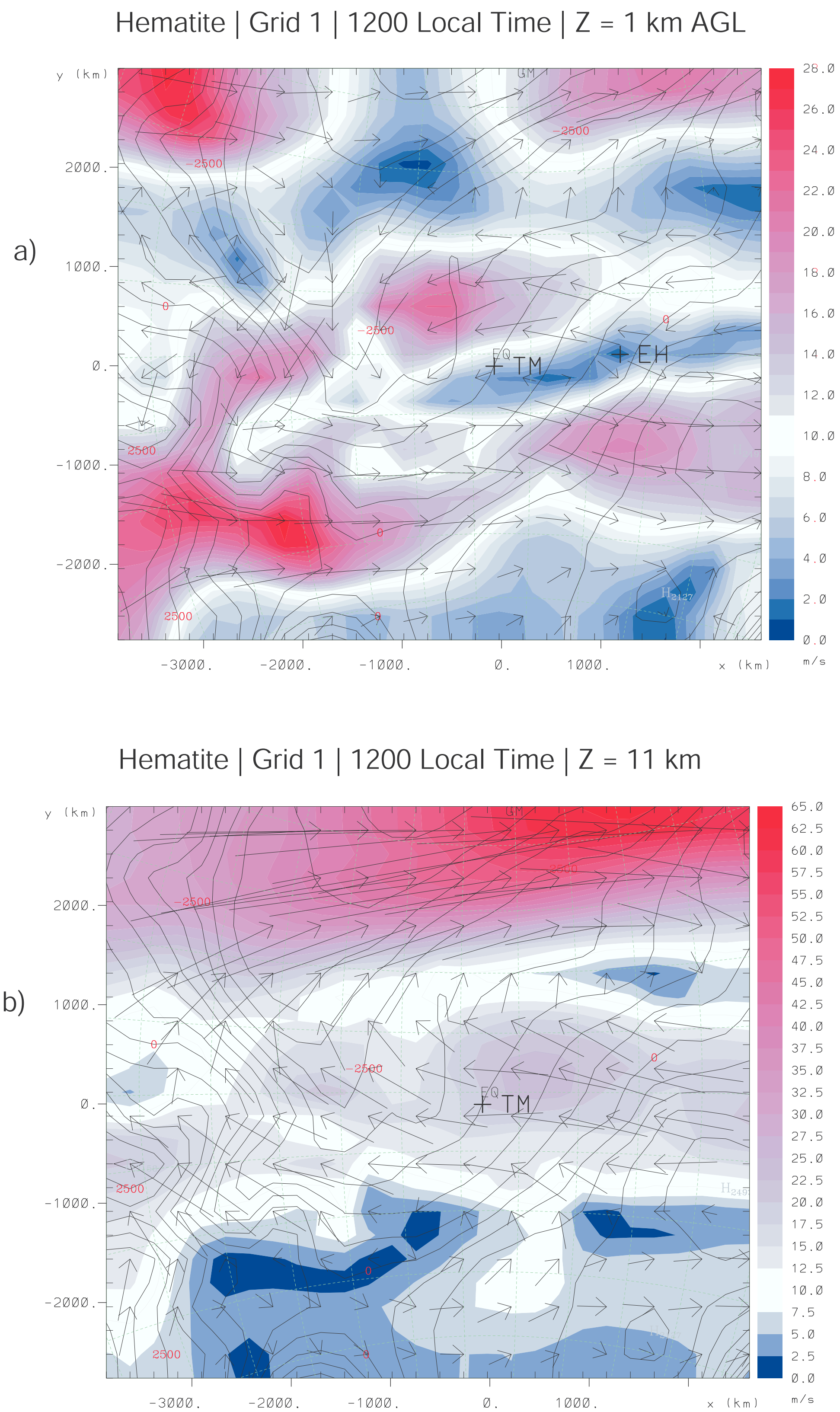

Figure 9. As in Figure 4, but for the Hematite landing site at (a) 1 km, and (b) 11 km. The East of Hematite site is also indicated in (a). See text for details.

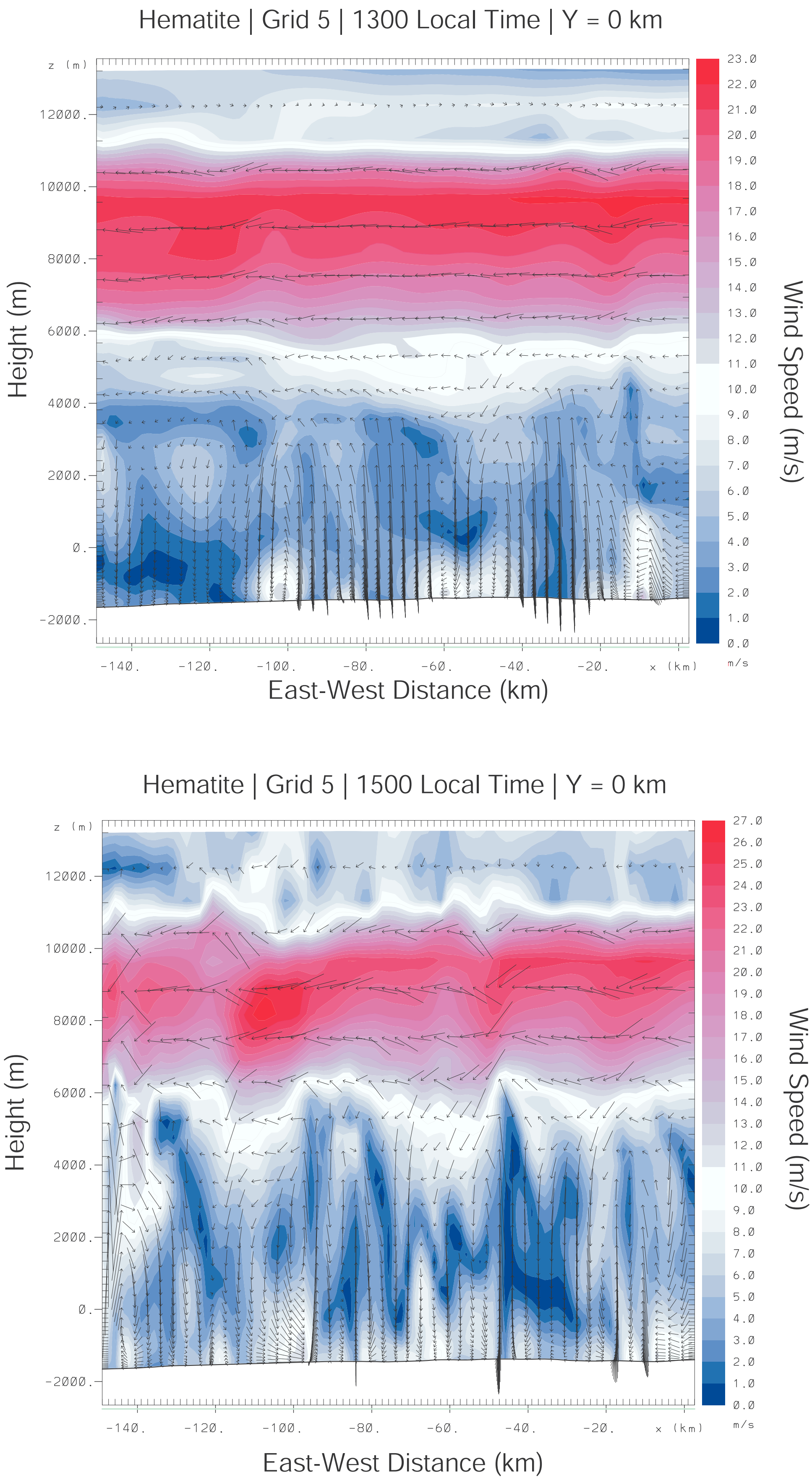

Figure 10. West-to-east vertical cross sections through the Hematite landing site on the fifth nested grid at (a) 1300 local time and (b) 1500 local time. The figure illustrates the thermal convection and growth of the boundary layer over the course of the afternoon.

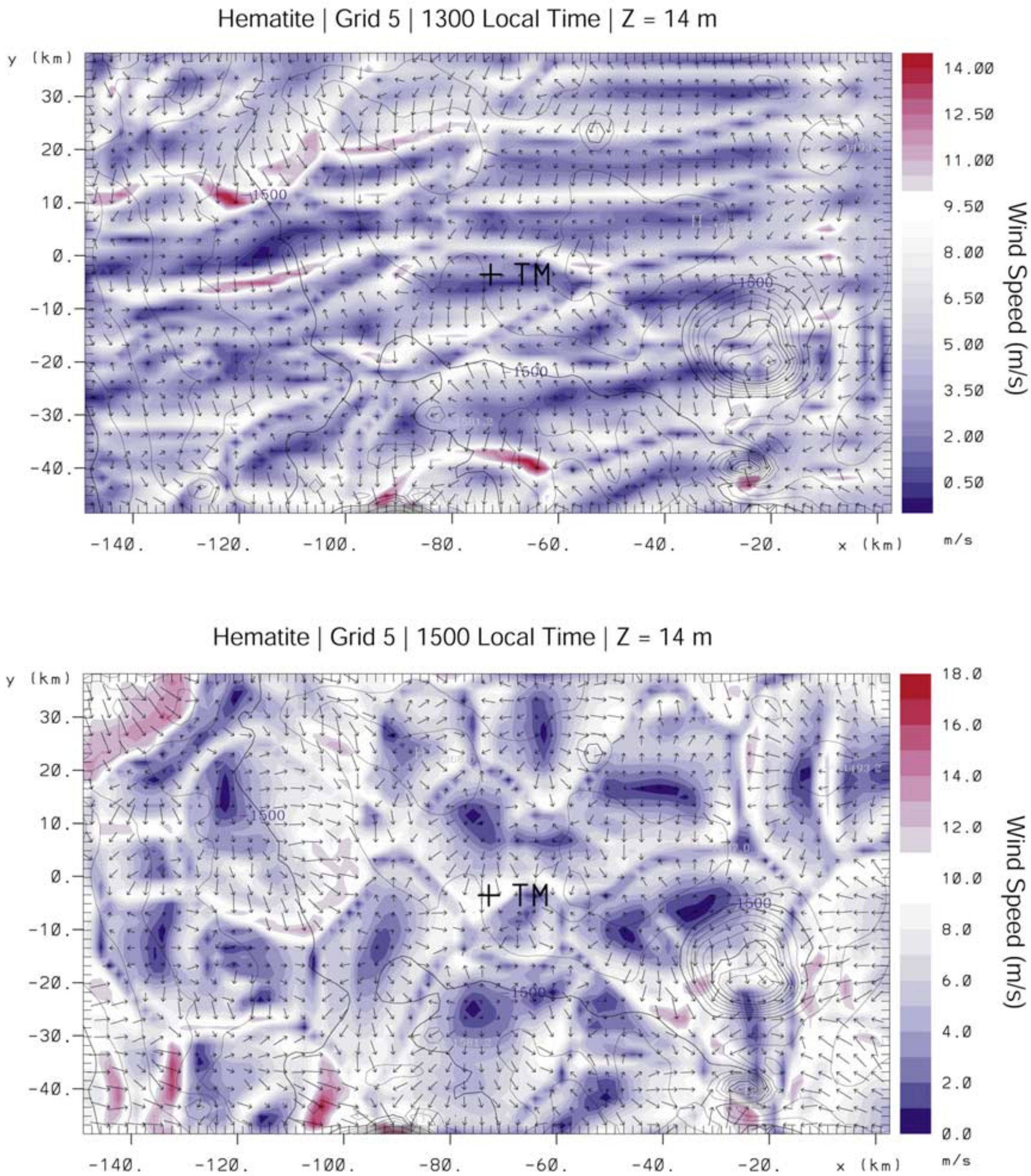

Figure 11. The early onset of convection on grid five in the Hematite simulations (a), and (b) the fully developed convective cell pattern later in the afternoon.

[37] The topography at this location (Figure 12a) reveals a crater roughly 400 km in diameter (about four times the size of Gusev crater). The rims are better defined in the eastern hemisphere of the crater. The coordinates specified for the center of the simulation are in the northeast portion of the crater about 20 km from the rim. The rim rises approximately 1 km above the surrounding terrain at this location.

[38] Although the crater is larger than Gusev crater, it exhibits many of the same circulation patterns. As the crater walls heat during the morning and afternoon, upslope flow diverging from the center of the crater is generated. The flow is strongest on the east rim due to enhancement by the approaching thermal tide. The eastern rim convergence boundary migrates significantly eastward from the ridge, but the western convergence boundary does not (Figure 12a). The western boundary does not appear to move into the crater later in the afternoon as it did in Gusev crater. Instead, the winds gradually diminish near sunset, and the boundary vanishes.

[39] A local peak near the site and along the crater rim interacts with the overnight and morning winds, which are katabatic easterly winds from Syrtis Major that blow over the crater (Figure 12b). The dense, stable air is partially blocked by the elevated topography along the west rim, especially at the local topographic peak. This creates a minimum in wind speed on the windward side of the rim. As discussed by *Magalhães and Gierasch* [1982], *Durran*

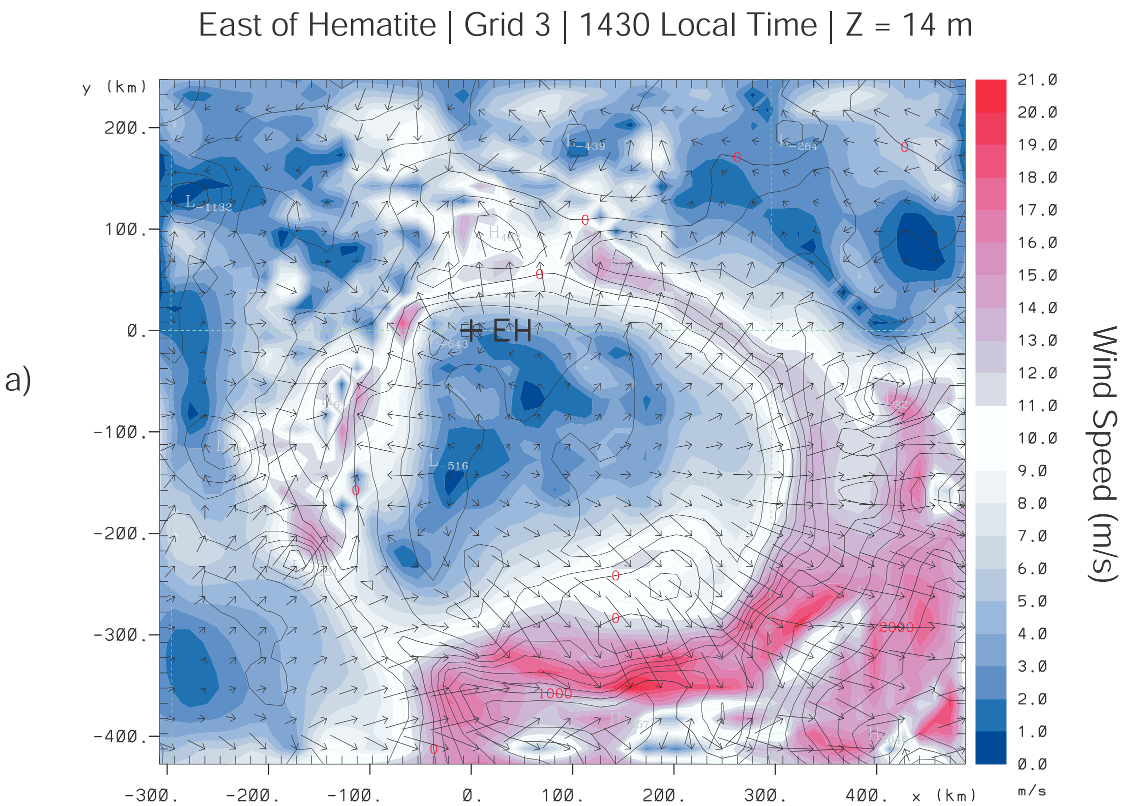

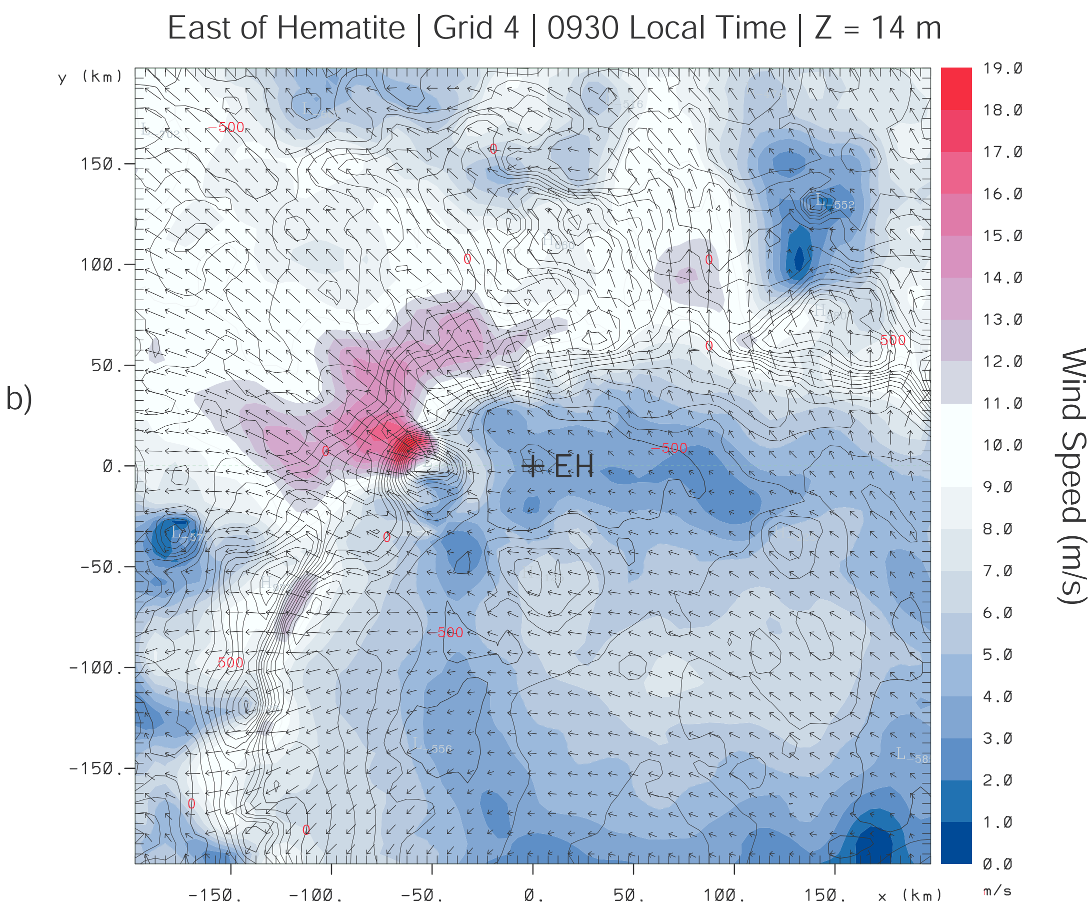

Figure 12. Near-surface atmospheric circulation at the East of Hematite site at (a) 1430 local time on the third grid, and (b) 0930 local time on the fourth grid. The third grid shows the location of the site (EH) relative to the crater basin.

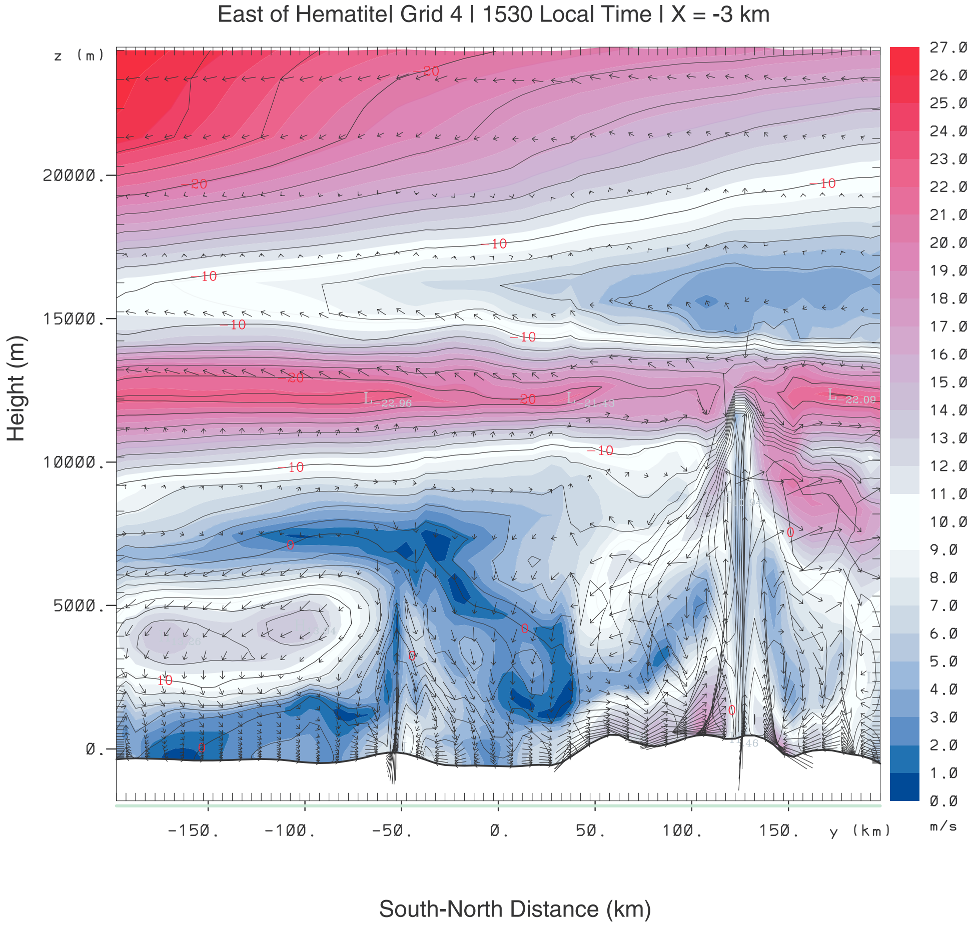

Figure 13. West-to-east vertical cross section at the East of Hematite site. Unlike Hematite, the convection is focused along topographic ridges, and the vertical extent of the convection can be greater in some locations. Wind speed is shaded; wind vectors are in the plane of cross section.

[1986], *Magalhães and Young* [1995], and *Rafkin et al.* [2001], the air is accelerated on the leeward side.

[40] The atmospheric structure and dynamics aloft are relatively simple. During the afternoon, convective plumes (Figure 13) are associated with elevated topographic features (hills). The winds below approximately 10 km are generally less than 10 ms^{-1} out of the northwest. A nearly uniform layer of stronger winds out of the southeast is present between 10 and 15 km AGL, although the speeds stay below 35 ms^{-1}. Occasionally, a few of the convective plumes penetrate into the layer of high winds.

3.4. Elysium Planitia and Elysium Edge

[41] The Elysium Planitia landing site is located between Elysium Mons to the northeast and the southern highlands to the southwest. During the daylight hours a strong low-level divergence pattern is established as the air moves toward these higher topographic regions. The landing site, being closer to the southern highlands, falls under the influence of the northerly upslope winds. The large-scale circulation near the surface is weak and completely masked by the much stronger mesoscale signature.

[42] At several thousand meters to 10 km above the reference areoid, light easterly winds dominate the area (not shown). At 10 km and higher, the landing site is located between the very intense tropical easterly jet and the middle-latitude westerly jet. However, the wind speeds generally remain less than 15 ms^{-1} (not shown).

[43] Convective circulation cells similar to those modeled at the Hematite location develop and strengthen throughout the afternoon with one important difference: The convection never develops beyond the linear structure into the well-defined hexagonal patterns (Figure 14). The persistent northerly wind suppresses the hexagonal structure. The strongest winds are at the leading edge of the thermal updrafts, which are aligned roughly with the mean wind shear vector over the depth of the convective boundary layer. With the exception of the regions immediately adjacent to the convective updrafts, wind shear is weak.

[44] Compared to previously discussed locations, the atmospheric environment and circulations are relatively benign. The convective thermals are slightly weaker than at Hematite, the mean wind appears slightly greater, and the wind shear is comparable.

[45] A second simulation was performed (named "Elysium Edge") centered on the ridge dividing Elysium Planitia and Isidis Planitia. This location is approximately 500 km to the northwest of the Elysium Planitia ellipse EP78B2.

[46] The results of the Elysium Edge simulation are nearly identical in character to the Elysium Planitia simu-

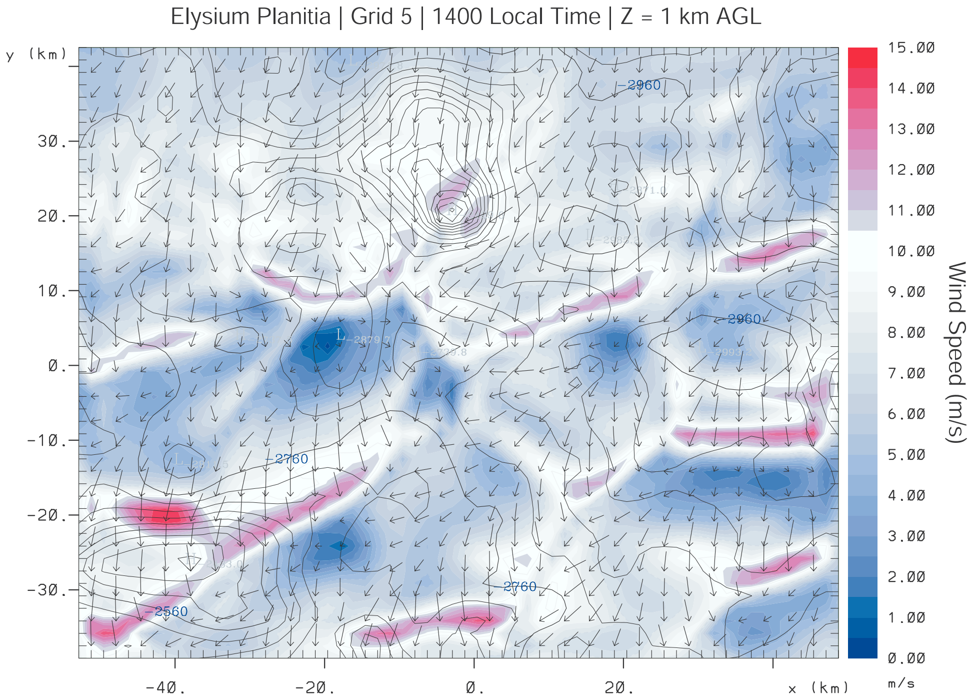

Figure 14. As in Figure 12, except for Elysium Planitia at 1400 local time, 1 km AGL, and on grid 5.

lation, except that the site is more strongly influenced by the southern highland thermal circulation and less strongly by the Elysium Mons circulation.

[47] During the afternoon, the upslope wind speeds are slightly under 10 ms^{-1}. These winds, which are slightly stronger than those at the Elysium Planitia site, further suppress the formation of hexagonal convective cells in favor of linear updraft structures (Figure 15a). A vertical cross section from south to north through the landing site (Figure 15b), reveals a well-defined northerly upslope layer in the lowest few kilometers. The wind speeds gradually increase from north to south. A gradual shift to southerly winds occurs approximately 2.5 km above the reference areoid. The highest magnitude ($\approx$20 ms^{-1}) winds are found at a height of approximately 11 km.

3.5. Isidis Planitia

[48] Isidis Planitia is a large impact basin on the eastern flank of Syrtis Major along the north-south topographic dichotomy. A large, broad ridge separates Isidis Planitia from Hellas basin to the south. The landing site in Isidis Planitia is located relatively close to the steep southern rim of the basin.

[49] The low-level flow is cyclonic at the scale of the basin during the morning and afternoon (Figure 16a). Air enters through the northernmost portion of the topographic saddle connecting the northern lowlands to the basin, circulates through the basin, and exits through the southwestern part of the saddle. In the morning, there is a low-level jet embedded within the central and southern portion of the circulation.

[50] The proximity of the landing site to the rim of the basin results in circulations with a strong upslope/downslope diurnal cycle. The upslope flows develop shortly after sunrise and are well developed by 1000 local time. As the upslope winds gradually strengthen with time, the low-level jet to the north of the site diminishes (Figure 16b). The greatest afternoon near-surface and boundary layer wind speeds (>25 ms^{-1}) are located on the southern crater rim near, but not at the proposed landing site.

[51] The relatively strong winds do not permit the development of organized hexagonal-like convective cells. Instead, the thermal convection organizes into weak shear-parallel updraft bands (Figure 16c). These linear features are oriented nearly north-south near the landing site and east-west to the northeast of the site.

[52] A north-south vertical cross section through the site reveals the atmospheric structure aloft (Figure 17). The upslope winds peak at approximately 1 km AGL. The most intense circulations are on the basin rim, where air is vented out of the basin. Turbulent kinetic energy in the upslope flow over the basin is less than 10 m^2s^{-2}, which suggests that the upslope flow is mildly turbulent. Over the rim, the turbulence increases dramatically. Above the upslope circulation is a well-defined return flow layer with moderate subsidence. The subsidence should suppress the growth of the afternoon convective boundary layer in a manner similar to that in Valles Marineris and Gusev Crater. The maximum depth of the convective boundary layer at the site is approximately 2.5 km, which is only one third of the height attained at the Hematite location.

4. Landing Site Surface Meteorology

[53] Although the main thrust of this paper is the meteorology at the time of EDL, landed operations can be impacted by meteorological conditions at all times of the sol. The most direct impact is probably the variations of temperature over time, which affect power consumption, particularly at night. In some instances strong winds may also impact operations by lifting dust and sand, obscuring visibility, and increasing heat loss due to increased ventilation.

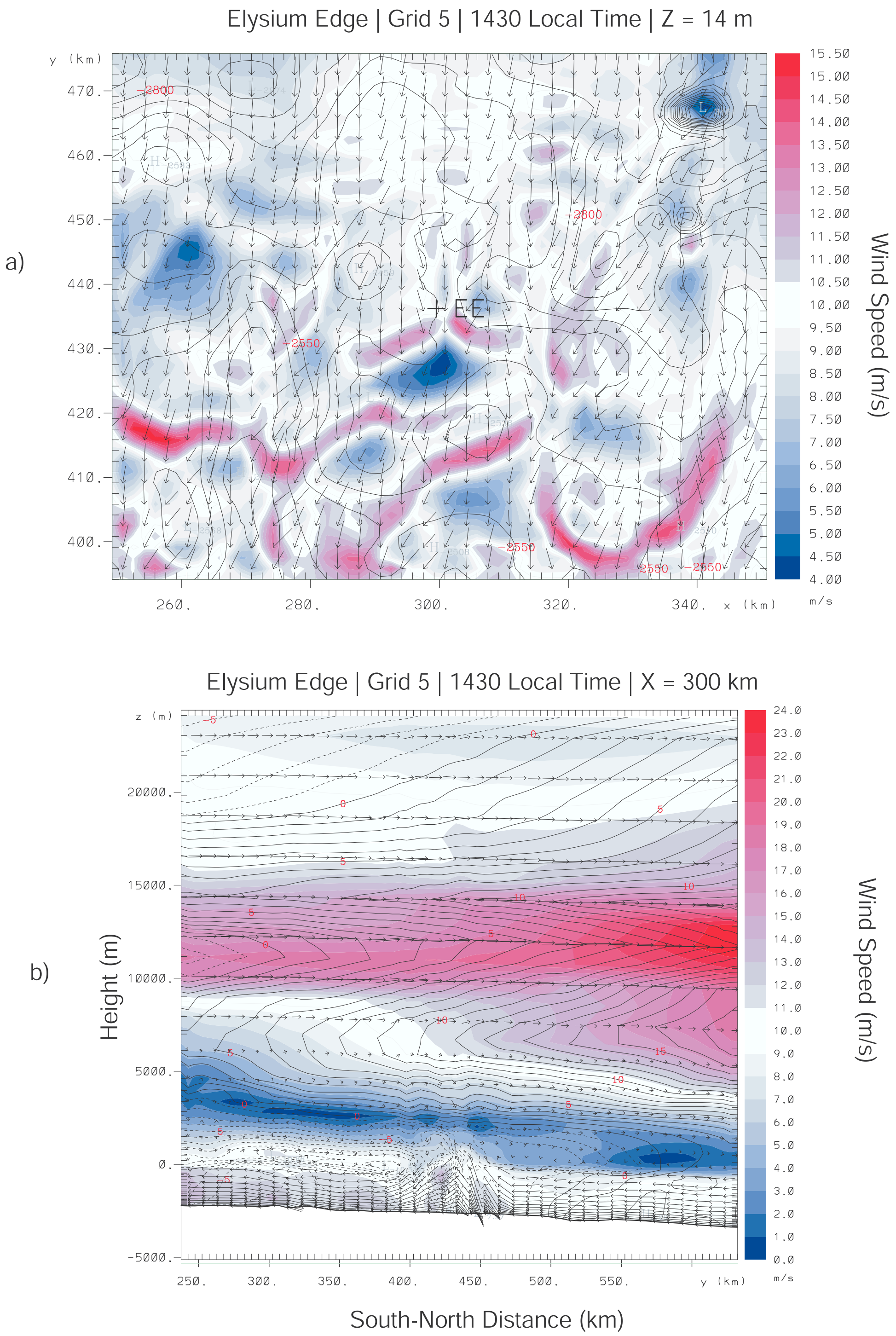

Figure 15. (a) Near-surface winds at Elysium Edge at 1430 local time, and (b) a south-to-north vertical cross section. The zonal wind (perpendicular to page) is contoured (negative dashed, positive solid).

[54] Figure 18 shows variations of temperature, wind speed, and direction for each of the previously described simulations. Note that the plotted values are point values taken at the center of the landing ellipse. Values surrounding the center of the ellipse can vary significantly from nearby areas within the ellipse. The temperature data have been reduced to a height of 1.5 m using surface layer theory scaling. No reduction has been made on the wind. Unfortunately, there will be no direct way of validating these data, as the landed science package contains no meteorological monitoring equipment.

[55] All of the sites show similar variations of temperature throughout a sol. Peak afternoon temperatures are near 270 K at the Valles Marineris landing site, which is the warmest location modeled. All of the locations remain above 180 K at night with the exception of the East of

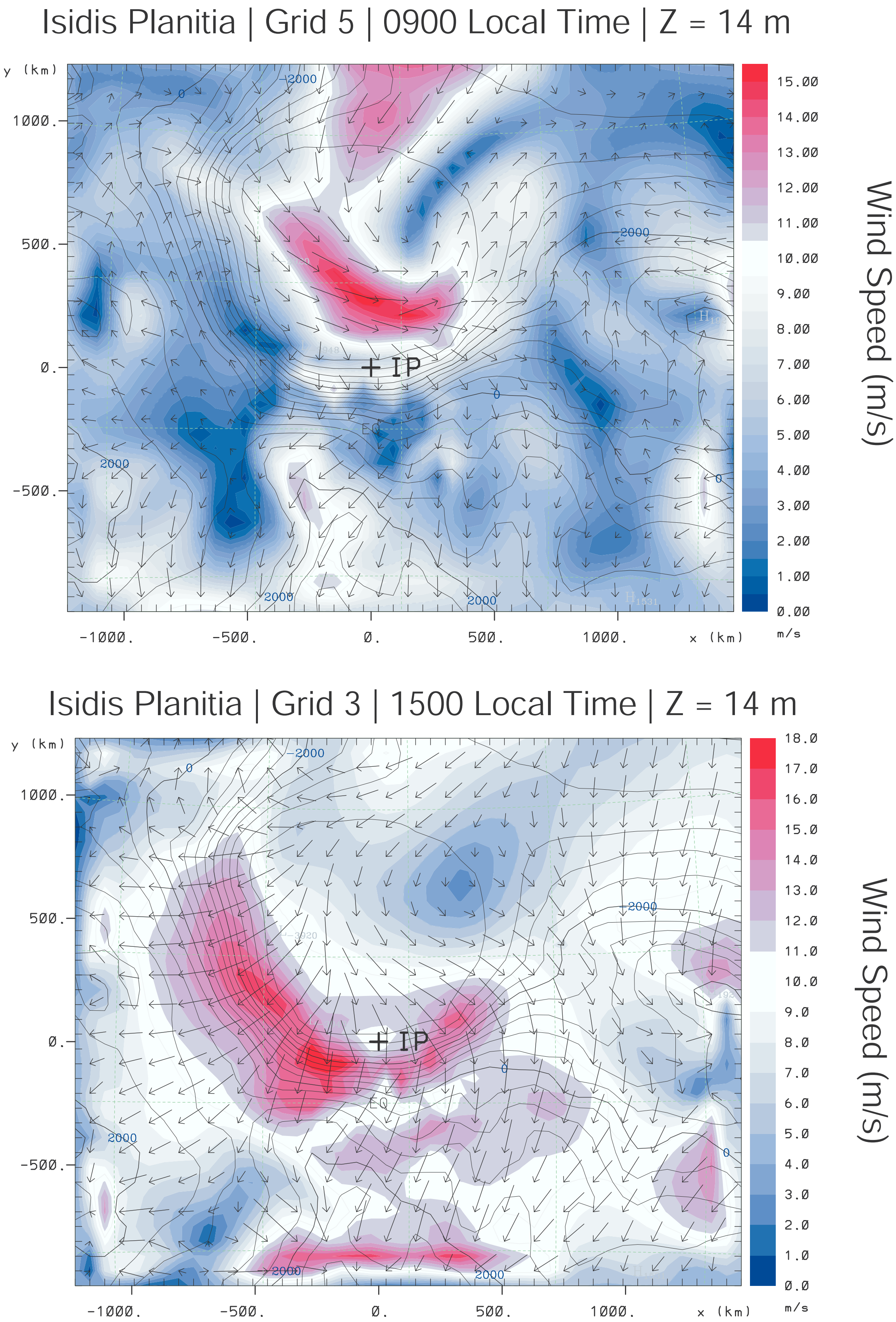

Figure 16. Atmospheric circulation patterns at Isidis Planitia on (a) grid 5 at 14 m and 0900 local time, (b) grid 3 at 14 m and 1500 local time, and (c) grid 5 at 14 m and 1500 local time. See text for details.

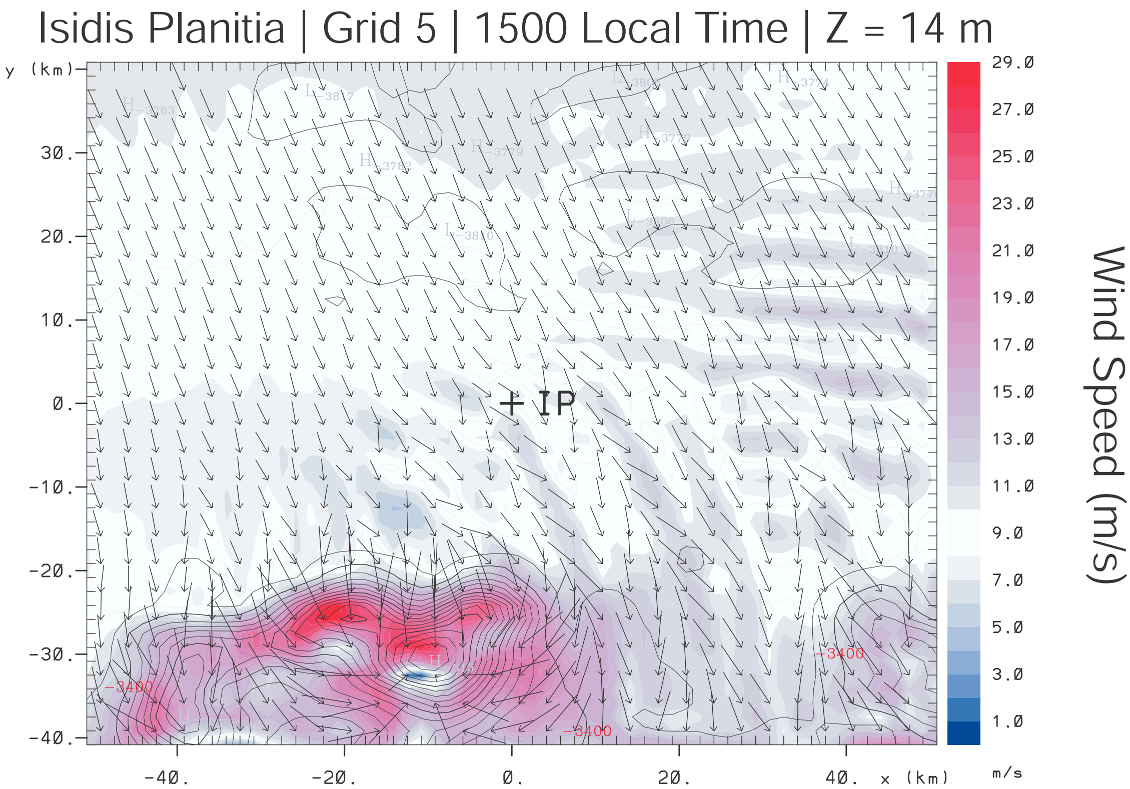

Figure 16. (continued)

Hematite location, which drops to near 160 K. All of the locations are persistently windy, even in the overnight hours.

[56] Valles Marineris has a striking pressure cycle. The diurnal variation of pressure is predicted to be slightly less than 200 Pa, or over 25% of the total pressure. The drop in pressure during the afternoon can be attributed to the venting of mass out of the canyon via upslope circulations, the contribution of thermal effects in reducing the hydrostatic pressure, and the pressure drop associated with the global tide. The pressure cycles at the other sites are not nearly as interesting and are not plotted.

5. Model Validity

[57] The validity of the MRAMS solutions at the proposed landing sites is a topic of great importance. The results are being used to provide input in the assessment of atmospheric hazards in the downselection of landing sites. Unfortunately, the paucity of meteorological data makes it almost impossible to quantitatively assess the model.

[58] Comparison of the MRAMS-predicted meteorology to that observed at the Mars Pathfinder landing site [*Rafkin et al.*, 2001; Michaels and Rafkin, submitted manuscript, 2002] and at Viking Lander 1 (T. I. Michaels and S. C. R. Rafkin, manuscript in preparation, 2003) have shown excellent agreement. Viking Lander 2 comparisons are ongoing and were the focal point for the mesoscale modeling session held at the Mars Atmospheric Modeling Intercomparison Workshop (Granada, Spain; January 2003). All of these sites are in topographically uninteresting locations. Consequently, there is no quantitative way of assessing model performance in topographically complex regions such as those found at many of the MER landing sites.

[59] Opportunities for qualitative measurements of model validity abound. Mars Orbiter Camera (MOC) images reveal numerous mesoscale dust and cloud circulations that provide insight into the underlying atmospheric structure and dynamics. The mesoscale modeling community has begun to take advantage of these images by attempting to simulate the observed features. For example, *Rafkin et al.* [2002] successfully simulated a dust spiral observed over Arsia Mons, and *Toigo and Richardson* [2002] have successfully simulated an observed dust front moving off of the edge of the polar cap. *Michaels and Rafkin* [2002] simulated convective circulations with characteristics that resemble observed convective cloud elements. *Kuzmin et al.* [2001] have found MRAMS simulations of flow over a crater consistent with erosion patterns of crater rims, and *Greeley et al.* [2003] have found correlations between MRAMS-predicted surface wind stresses and the geomorphology of dunes within Gusev crater. The ability of these models to qualitatively reproduce observed atmospheric structures and their ability to predict atmospheric flows consistent with geologic interpretation enhances their credibility in regions of complex terrain where standard meteorological data are nonexistent.

[60] All of the mesoscale models currently in use for Mars are derivatives of Earth-based simulation code, which have been used successfully for almost three decades. The underlying physics (i.e., fluid dynamics) of the atmospheres of Mars and Earth (and all planetary atmospheres) are fundamentally the same, although the physics may be expressed differently as a result of variations in forcing.

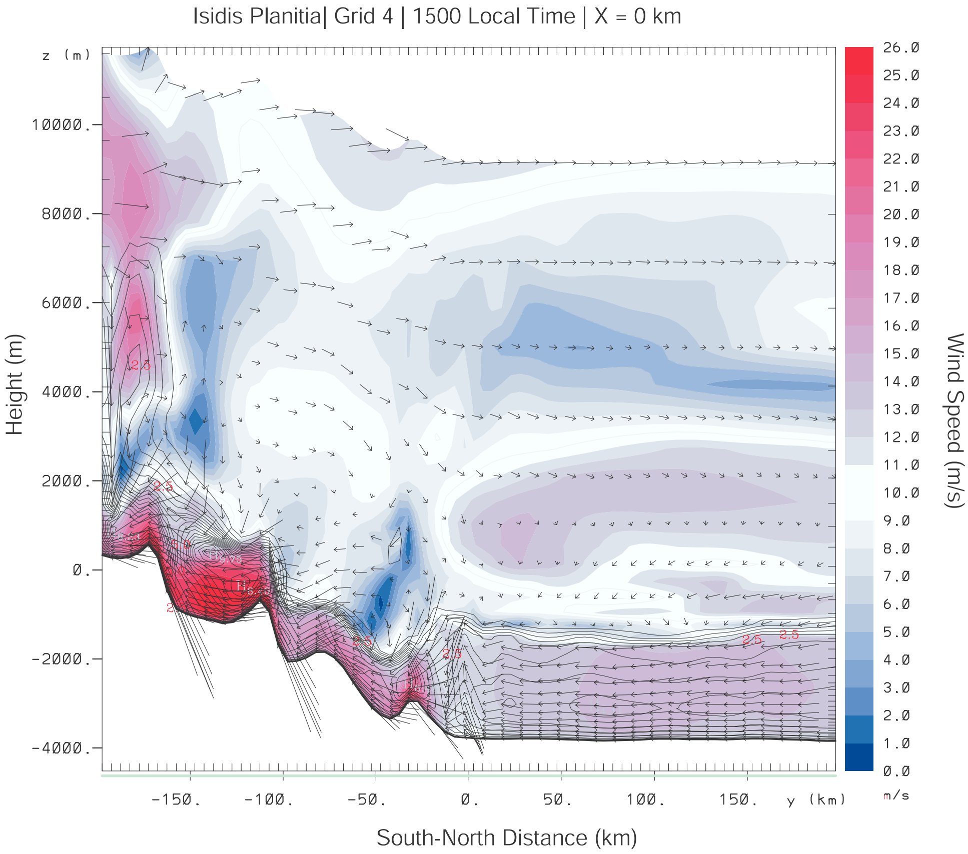

Figure 17. South-to-north vertical cross section on grid four through the Isidis Planitia landing site. Subgrid-scale TKE is contoured. See text for details.

[61] Earth simulations are not always accurate. The Earth's near-surface atmosphere has a longer radiative time constant and is more massive than Mars', which results in much weaker thermal circulations for a given gradient in heating. Consequently, mesoscale circulations in the Earth's atmosphere tend to be more strongly controlled by large-scale forcing and by mechanical forcing from topographic relief. Errors in model initialization and boundary conditions can produce spurious results in Earth simulations, and often contribute significantly to total model error. These complications are greatly reduced in the modeling of Mars' atmosphere, which should in principle result in greater simulation accuracy. Consequently, to the extent that Earth simulations are successful, there are expectations that the same core model dynamics and numerics are able to capture Mars' atmospheric dynamics given proper forcing.

[62] Given the inability to directly validate the model data at the landing sites, and given the potentially large impact that the data might have on landing site selection, the model results were presented to an atmospheric panel review board convened specifically to determine the level of confidence of the data. Furthermore, simulation results from the Mars MM5 model [*Toigo and Richardson*, 2003] were also presented. The MRAMS and MM5 simulations were conducted independently.

[63] The review board determined that the results from the models were consistent with the known dynamic response of the Martian atmosphere to heating and topographic forcing, and that models can provide meaningful guidance on atmospheric wind hazards.

6. Discussion

[64] Qualitatively, each of the landing sites appears to pose at least some risk to EDL. In some cases, particularly in Valles Marineris, the level of risk due to strong winds and wind shear appears significant enough that quantitative analysis is almost unnecessary. Other locations, such as Hematite, Isidis Planitia, and Elysium Planitia, require quantitative analysis in order to properly assess the risk due to atmospheric hazards.

[65] Reduction of these model data to a form usable by mission planners and engineers is not a trivial matter. The output from the atmospheric models is not directly compatible with the engineering models used to assess spacecraft performance or risk. K03 describe in detail the methods by which these model data were interfaced with the engineering models in order to provide a quantitative assessment of each of the landing sites.

[66] Several important items have become clear from the simulations. First, any assumptions about quasi-persistent mean winds or generalizations based on large-scale mean winds or average winds (such as those provided by general circulation models) would be grievously in error, particularly in regions of complex topography. Second, the Martian atmosphere is extremely energetic on the mesoscale or smaller, except perhaps at night at locations on the plains

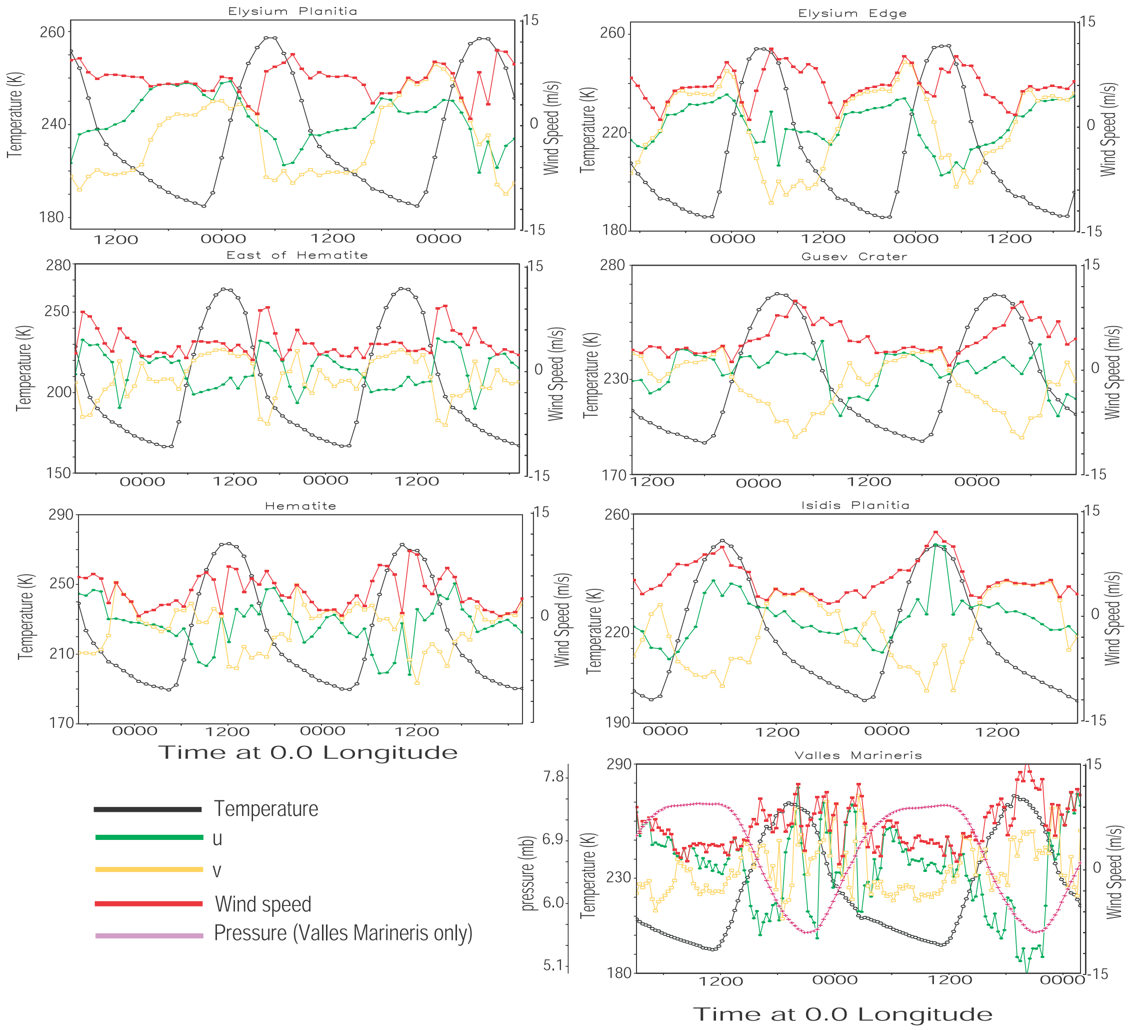

Figure 18. Time series of meteorological parameters over roughly a two sol period for the seven modeled landing sites.

far away from katabatic source regions. Third, when heated, the atmosphere of Mars transports thermal energy by two dominant mechanisms: free convection and topographic venting. Finally, it is now clear that additional in situ meteorological observations of the Martian atmosphere are needed.

[67] On the basis of numerous modeling studies, including those presented here, it appears that Mars is a windy place. Its low atmospheric density and intense radiative processes drive robust thermal circulations during the day and night. There are typically only a few short hours during the period of transition from upslope to downslope flow (and vice versa) when the winds slacken. Occasionally, the wind reversals come in the form of a katabatic front, and the wind speeds do not diminish at all. Meteorological data from the three landed missions (Viking 1 and 2, and Mars Pathfinder) may have produced a false sense of security about wind hazards and, in the case of Mars Pathfinder (MPF), about the ability of passive landing systems, such as parachutes and air bags, to successfully land. Until recently, the lack of mesoscale model data and the availability of large-scale general circulation model data have perhaps contributed to the false impression that local winds and wind speeds can be characterized by the spatially and often time-averaged winds generated by general circulation models. General circulation models provide important information on where to begin looking, but mesoscale circulations can be fierce in regions that look benign on the large-scale.

[68] Simulations of the MPF landing site conducted as part of the panel review process suggested that MPF landed in an optimal location in the lee of a streamlined landform that blocks the nighttime katabatic flows from Ares Vallis to the south. Had the MPF spacecraft landed just a few kilometers east or west and an hour or two later, it may have been subjected to substantially higher winds. Significant portions of the MPF landing ellipse are subjected to these katabatic flows. The MPF EDL was (obviously) successful, and the success was the main driving force for the utilization of the system for MER. However, it should not be assumed that such a system is appropriate for landing at a wide variety of locations and times based solely on one successful landing. Furthermore, it should not be assumed that the night is any less hazardous than the daytime.

[69] On the basis of the numerical model simulations of thermal convection, the influence of winds, and the influence of topography, there is enough information to broadly

predict the atmospheric structure at locations prior to simulation. This is important, as the modeling studies are computationally expensive. In places with flat topography, free convection dominates in the afternoon. Convection organizes into hexagonal cells in environments with weak winds and low wind shear. As wind speed and shear increase, the cells elongate and become linear. When topography is present, air rises preferentially along the slopes. In some cases, compensating subsidence further suppresses free convection, and results in the topographic venting that may account for nearly all the vertical heat and mass transport.

[70] Determining atmospheric structure is particularly important for passive landing systems such as that used by the MER. Mesoscale models provide one tool for providing at least reasonable expectations of what a landing spacecraft might encounter. However, there still remains a fundamental issue: mesoscale models have not been validated except at less than a handful of sites where observations are available. Atmospheric structure and dynamics issues aside, there are real engineering needs for ground-based atmospheric measurements on Mars. Validating the models with measurements from only a few more locations (especially in regions of complex topography) would significantly increase the confidence in the models in places where observations are unavailable. In return, hazardous locations could be identified and avoided, or systems designed to overcome the hazards could be developed.

[71] Without directly quantifying the effect of the atmosphere on EDL, it is still possible to qualitatively identify the most likely hazards directly from the model data, even if the magnitude of the hazard is not calculated. The discussion of these hazards for each of the locations follows.

6.1. Valles Marineris

[72] Valles Marineris appears to be the most hazardous of all the landing sites. The greatest threat to the lander appears to be the magnitude of the winds, although there is often moderate wind shear throughout the inversion. Vertical winds are strong near the edge of the canyon, but the proposed landing ellipses are far enough away from the walls so that this hazard is minimal. Turbulent kinetic energy indicates that there is significant atmospheric energy at scales of a few hundred meters and less.

[73] The timing of EDL in Valles Marineris would be of great importance. An EDL at the later end of the window would increase the likelihood that the spacecraft would encounter low-level easterly winds, shear, and turbulence of catastrophic magnitude. There are some locations that are protected from these strong winds, but the regional scale of these locations is an order of magnitude smaller than the 3σ landing ellipse.

[74] Even if it were possible to accurately target a small, wind-protected landing site, the spacecraft would still have to deal with strong wind shear and small-scale turbulence during descent.

6.2. Hematite and East of Hematite

[75] The simulation of the Hematite landing site suggests that the greatest atmospheric hazards to EDL are the wind gusts, wind shear, and potentially the large vertical velocities associated with the convective thermal circulations. The mean wind speeds and shear are relatively benign with the possible exception of the upper-level easterly jet.

[76] Should the spacecraft descend directly through the core of an updraft or downdraft, the retrorockets should be able to compensate for the velocity, provided that the rate of change of velocity prior to radar termination is a good predictor for vertical velocity after radar termination. For example, if the updraft and downdraft velocity gradients are linear, then extrapolation would be sufficient.

[77] Another plausible scenario is that the spacecraft will descend or pass through the edge of an updraft plume. Such a path might result in extrapolation errors of the vertical velocity. There may also be aerodynamic forces, the magnitude of which are unknown to the authors, that could lower the performance of the parachute as it passes in or out of the updraft core. Such forces are well known, for example, to glider pilots that seek out and penetrate thermals; differential lift across the wings will cause the plane to roll.

[78] The East of Hematite simulation appears outwardly similar to those of Isidis Planitia, Elysium Planitia, and Elysium Edge. Convective circulations are evident, but the mean wind and wind shear suppress hexagonal structures in favor of linear organization. Mesoscale thermal circulations associated with the large crater are strongly expressed in the total wind.

6.3. Gusev Crater

[79] Model predictions at Gusev crater indicate a very transient atmospheric structure. Among all the sites, Gusev crater probably illustrates most clearly why large-scale information is insufficient for identifying atmospheric hazards. Although the intense thermal circulations associated with the crater might have been anticipated, it is unlikely that the interaction of the tide with the mesoscale circulation would have been contemplated.

[80] The landing system can correct for moderate wind speeds and wind shear, but the simulated atmospheric conditions at Gusev crater suggest that wind speed and perhaps wind shear may exceed the level of tolerance for EDL.

6.4. Isidis Planitia

[81] The most significant hazard at Isidis Planitia appears to be the mean wind. Turbulence, wind speed, and wind shear increase at locations closer to the rim of the basin. EDL in the late morning may be more hazardous than in the early afternoon due to the presence of the low-level jet in the southern and central part of the basin.

6.5. Elysium Planitia and Elysium Edge

[82] The Elysium Planitia and Elysium Edge sites possess a combination of potential hazards. The hazards associated with free atmospheric convection discussed at the Hematite location are present. Additionally, there is a moderate mean wind and some wind shear layers that may approach or exceed desired levels. The mean wind appears comparable to that at Isidis Planitia.

[83] If the EDL system can handle the convection, the Hematite location would seem preferable to the Elysium sites since Hematite appears to have lower mean wind and

wind shear. If the system is unable to handle the convection, then Isidis Planitia may be more desirable since the free convection is more suppressed than at Elysium.

7. Summary and Conclusion

[84] The MER mission utilizes an airbag landing system based on the successful MPF mission. The system is sensitive to the mean wind and wind shear, and potentially sensitive to vertical air currents (convection). At present, mesoscale models provide the only means by which to reasonably estimate the atmospheric hazards at potential landing sites. Mesoscale models, including MRAMS, appear to be valid on the basis of limited quantitative observations, widely available qualitative observations (images), and inference from the success of Earth mesoscale models. The results presented here were reviewed by a special panel and were found to be reasonable and consistent with known atmospheric dynamics.

[85] The meteorology during the EDL window at most of the sites is dynamic. The intense heating of the lower atmosphere drives intense thermals and mesoscale thermal circulations. Moderate mean winds, wind shear, turbulence, and vertical air currents associated with convection are present and potentially hazardous to EDL. Some locations qualitatively appear to approach (Gusev Crater) or exceed (Valles Marineris) acceptable levels of tolerance. Other locations require quantitative analysis in order to characterize the hazard level.

[86] Atmospheric hazards associated with local meteorology ought to be given a higher level of priority earlier in the landing site selection process. More robust or controlled landing systems (such as in the Viking missions) might be sufficient to overcome a wider range of atmospheric hazards and open up a greater variety of terrain for exploration. Or, the passive landing systems must be designed so as to withstand stronger winds and wind shear. Yet another solution is to invert the problem: decide where to go first and then design a system that can tolerate the environment. Passive landing systems that employ this inverted problem would greatly minimize risk.

[87] Current observational techniques and large-scale circulation models are generally not sufficient for identifying local atmospheric hazards. Large-scale data are important for identifying regions where synoptic-scale circulations and winds are favorable, and the data are required for the initialization and boundary conditions that drive the mesoscale models. Thus large-scale data and general circulation models play a key and absolutely critical role in hazard identification. Neither mesoscale models nor general circulation models are sufficient individually. Finally, in situ measurements are desperately needed. Science return aside, the data can be used to validate and improve the models, which would make definitive atmospheric hazard assessment a more tractable problem.

[88] **Acknowledgments.** The authors are grateful to the MER JPL team and Dr. Joy Crisp in particular for their support of this research. The authors would also like to thank Dr. Alison Bridger, Dr. Anthony Colaprete, Dr. Robert Haberle, Dr. David Kass, Dr. Jeff Hollingsworth, and the model review committee for their insightful comments and discussions. The authors would also like to thank the two anonymous reviewers, whose comments greatly improved this paper.

References

Crisp, J. A., M. Adler, J. R. Matijevic, S. W. Squyres, R. E. Arvidson, and D. M. Kass, Mars Exploration Rover mission, *J. Geophys. Res.*, *108*(E12), doi:10.1029/2002JE002038, in press, 2003.

Durran, D. R., Mountain waves, in *Mesoscale Meteorology and Forecasting*, edited by P. S. Ray, pp. 472–492, Am. Meteorol. Soc., Boston, Mass., 1986.

Greeley, R., R. O. Kuzmin, S. Rafkin, T. Michaels, and R. M. Haberle, Wind-related features in Gusev crater, Mars, *J. Geophys. Res.*, *108*(E12), doi:10.1029/2002JE002006, in press, 2003.

Kass, D., J. T. Schofield, T. Michaels, S. Rafkin, M. Richardson, and A. Toigo, Analysis of atmospheric mesoscale models for entry, descent, and landing, *J. Geophys. Res.*, *108*(E12), 8090, doi:10.1029/2003JE002065, in press, 2003.

Kuzmin, R. O., R. Greeley, S. C. R. Rafkin, and R. M. Haberle, Wind-related modification of some small impact craters on Mars, *Icarus*, *153*, 61–70, 2001.

Magalhães, J. A., and P. Gierasch, A model of Martian slope sinds: Implications for aeolian transport, *J. Geophys. Res.*, *87*, 9975–9984, 1982.

Magalhães, J. A., and R. E. Young, Downslope windstorms in the lee of ridges on Mars, *Icarus*, *113*, 277–294, 1995.

Michaels, T. I., Large eddy simulation of atmospheric convection on Mars, thesis, San Jose State Univ., San Jose, Calif., 2002.

Pielke, R. A., et al., A comprehensive meteorological modeling system: RAMS, *Meteorol. Atmos. Phys.*, *49*, 69–91, 1992.

Rafkin, S. C. R., R. M. Haberle, and T. I. Michaels, The Mars Regional Atmospheric Modeling System (MRAMS): Model description and selected simulations, *Icarus*, *151*, 228–256, 2001.

Rafkin, S. C. R., M. R. V. Sta. Maria, and T. I. Michaels, Simulation of the atmospheric thermal circulation of a Martian volcano using a mesoscale numerical model, *Nature*, *419*, 697–699, 2002.

Toigo, A. D., and M. I. Richardson, A mesoscale model for the Martian atmosphere, *J. Geophys. Res.*, *107*(E7), 5049, doi:10.1029/2000JE001489, 2002.

Toigo, A., and M. Richardson, Meteorology of proposed Mars Exploration Rover landing sites, *J. Geophys. Res.*, *108*(E12), 8092, doi:10.1029/2003JE002064, in press, 2003.

Tyler, D., J. R. Barnes, and R. M. Haberle, Simulation of surface meteorology at the Pathfinder and VL1 sites using a Mars mesoscale model, *J. Geophys. Res.*, *107*(E4), 5018, doi:10.1029/2001JE001618, 2002.

T. I. Michaels and S. C. R. Rafkin, Department of Space Studies, Southwest Research Institute, 1050 Walnut Street, Suite 400, Boulder, CO 80302, USA. (srafkin@boulder.swri.edu)